Dear Todd Ehlers,

Thank you very much for the review. We included the suggested revisions into the manuscript.

This manuscript received two thorough and thoughtful reviews that identified areas of the manuscript where clarification was needed. Both reviewers are experts in either the field of bioturbation and landscape modeling approaches. The primary areas where changes were requested included: a) clarification of the 'new' aspects of the study and improved comparisons to previous work; b) more precise presentation of results in figures and associated text; and c) improved presentation of the modeling approach used.

The authors have done a thorough job addressing the reviewer's comments, and I thank them for the detailed response to reviews and figure/table/ and text revisions. The text (and figure changes) presented in response to reviews nicely address the reviewer's comments - and represent substantial revisions.

Unfortunately, (not the author's fault) I didn't see an uploaded version of the revised manuscript text and figures on the website. I realize the Copernicus website doesn't explicitly ask for this. However, many authors often included the full revised manuscript (with track changes) at the end of their review response. Given this, I kindly ask the authors to upload (after some minor suggestions I make below) the revised version of their manuscript and figures (with track changes for the text) to the website. This version should include the changes indicated in their response to reviews. If the authors did not track changes during revisions, then they can (in MS Word at least) use the option to difference the revised and original versions of the text to have a succinct summary of changes.

We provide the manuscript with all track changes highlighted in green below this rebuttal letter.

Two additional (minor) changes I ask the authors to make:

First, the text (and response to reviews) repeatedly says "Machine Learning" techniques were used for upscaling observations. I didn't see an explanation of how this was done in the text or supplemental material. As there are many, many, many different machine learning approaches, I ask the authors to revise the text associated with this to explain what technique was used. What the inputs were, what the outputs from this are, and how the algorithm was trained (if relevant). A reference(es) for the technique used should also be given. The relevant equations should be given if the approach is new. When making these changes, please keep in mind that readers of the manuscript should have sufficient knowledge of what you did so that they could reproduce your approach.

We have rewritten the section describing the estimation of spatial parameters and put more emphasis on applied the machine learning methodology:

Lines 447 – 464: For spatial parameterization of the DMMF model, we predicted land cover, soil properties and burrow distribution onto the hillslope catchments using machine learning techniques. We used the approach Meyer et al. 2018. The most important predictors were selected by forward feature selection. The quality of the random forest models was assessed by Leave-Location-Out cross validation. We trained the model stepwise, using in-situ data collected from seven of the hillslope catchments and validated the model using in-situ data from the remaining hillslope catchment (Meyer et al., 2018). The prediction was done at 0.5 m spatial resolution. We used the WorldView-2 layers obtained with a single license from GAF, NDVI, DEM, DSM, slope and roughness as predictors. The PAN-sharpening of the WV-2 layers was done by GAF.

For the area-wide prediction of burrow locations across the hillslope catchments, we used the burrow presence and absence data (section 3.1) as the response data within the RF models. The accuracy was 0.82 for PdA, 0.77 for SG, 0.75 for LC and 0.85 for NA. The prediction of soil properties was done using soil properties estimated along the track line (see section 3.1) as response data within the RF models. All of the models reached a high accuracy (see Table A1).

To obtain land cover classification, we used as the response within the RF models the land cover measured in-situ. The classes were soil without rocks, rocks, biocrusts, grass/herbs, shrubs and trees. Predictor values for each class were extracted from at least 100 polygons per site and class. The accuracy of the RF models was 0.71 for PdA, 0.81 for SG, 0.83 for LC and 0.75 for NA.

Second, please add a statement in the acknowledgments (or main text) about where the data and models used in the study can be accessed. For example, is there a link (or DOI preferably) for the source code and data used in the study? Please also do this for the machine-learning code used. Data or software archiving (with a DOI) can easily be done through https://zenodo.org or via GFZ data services (for EarthShape related research) - note however, the copyright of the erosion modeling software used must be honored and you may not be allowed to repost it (hopefully not).

We included in the acknowledgments where the data used, model output and model code can be accessed:

Lines 826 – 829: Code/Data availability: The estimated soil properties (DOI: 10.5678/wsrb-9f70), modelled sediment redistribution (DOI: 10.5678/32wa-d179) and model code (https://gitlab.uni-marburg.de/fb19/ag-bendix/model-sediment-redistribution-caused-by-bioturbating-animals) was published via LCRS data services.

Mammalian bioturbation amplifies rates of both hillslope sediment erosion and accumulation along Chilean climate gradient

Paulina Grigusova[1], Annegret Larsen[2], Roland Brandl[3], Camilo del Río[4,5], Nina Farwig[6], Diana Kraus[6], Leandro Paulino[7], Patricio Pliscoff[4,8,9], Jörg Bendix[1]

[1] Laboratory for Climatology and Remote Sensing, Department of Geography, University of Marburg, 35037 Marburg, Germany; paulina.grigusova@staff.uni-marburg.de (P.G.); bendix@geo.uni-marburg.de (J.B.)

[2] Soil Geography and Landscape, Department of Environmental Sciences, Wageningen University & Research, 6700 AA Wageningen, The Netherlands; annegret.larsen@wur.nl

[3] Animal Ecology, Department of Biology, University of Marburg, 35032 Marburg, Germany; brandlr@biologie.uni-marburg.de

[4] Facultad de Historia, Geografía y Ciencia Política, Instituto de Geografía, Pontificia Universidad Católica de Chile, 782-0436 Santiago, Chile; cdelriol@uc.cl

[5] Centro UC Desierto de Atacama, Pontificia Universidad Católica de Chile, 782-0436 Santiago, Chile

[6] Conservation Ecology, Department of Biology, University of Marburg, 35047 Marburg, Germany; diana.kraus@biologie.uni-marburg.de (D.K.); nina.farwig@biologie.uni-marburg.de (N.F.)

[7] Facultad de Agronomía, Universidad de Concepción, 3780000 Chillán, Chile; lpaulino@udec.cl

[8] Facultad de Ciencias Biológicas, Departamento de Ecología, Pontificia Universidad Católica de Chile, 8331150 Santiago, Chile; pliscoff@uc.cl

[9] Center of Applied Ecology and Sustainability (CAPES), Pontificia Universidad Católica de Chile, 8331150 Santiago, Chile; pliscoff@uc.cl

Corresponding author:

Paulina Grigusova

paulina.grigusova@staff.uni-marburg.de

Abstract

Animal burrowing activity affects soil texture, bulk density, soil water content and redistribution of nutrients. All of these parameters in turn influence sediment redistribution, which shapes the earth surface. Hence it is important to include bioturbation into hillslope sediment transport models. However, the inclusion of burrowing animals into hillslope-wide models has thus far been limited, and largely omitted vertebrate bioturbators, which can be major agents of bioturbation, especially in drier areas. Here, we included vertebrate bioturbator burrows into a semi-empirical Morgan-Morgan-Finney soil erosion model to allow a general approach to for assessing the impacts of bioturbation on sediment redistribution within four sites along the Chilean climate gradient. For this, we predicted the distribution of burrows by applying machine learning techniques in combination with remotely sensed data into the hillslope catchment. Then, we adjusted the spatial model parameters at predicted burrow locations based on field and laboratory measurements. We validated the model using field sediment fences. We estimated the impact of bioturbator burrows on surface processes. Lastly, we analyse how the impact of bioturbation on sediment redistribution depends on the burrow structure, climate, topography, and adjacent vegetation.

Including bioturbation greatly increased model performance and demonstrates the overall importance of vertebrate bioturbators in enhancing both sediment erosion and accumulation along hillslopes, though this impact is clearly staggered according to climatic conditions. Bioturbation had contrasting effects on sediment redistribution in arid than in semi-arid and Mediterranean, as well as in humid climate zone. Burrowing vertebrates increased sediment accumulation by 137.8 % ±16.4 % in the arid zone (3.53 kg ha^{-1} year^{-1} vs. 48.79 kg ha^{-1} year^{-1}), sediment erosion by 6.5 % ±0.7 % in the semi-arid zone (129.16 kg ha^{-1} year^{-1} vs. 122.05 kg ha^{-1} year^{-1}) and sediment erosion by 15.6 % ±0.3 % in the Mediterranean zone (4602.69 kg ha^{-1} year^{-1} vs. 3980.96 kg ha^{-1} year^{-1}). Bioturbating animals seem to play only a negligible role in the humid zone. Within all climate zones, bioturbation did not uniformly increase erosion or accumulation within the whole hillslope catchment. This depended on adjusting environmental parameters. Bioturbation increased erosion with increasing slope, sink connectivity and topography ruggedness, decreasing vegetation cover and soil wetness. Bioturbation increased sediment accumulation with increasing surface roughness, soil wetness and vegetation cover.

1. Introduction

Bioturbation was shown to shape the land surface (Hazelhoff et al., 1981; Istanbulluoglu, 2005; Taylor et al., 2019; Tucker and Hancock, 2010; Whitesides and Butler, 2016; Wilkinson et al., 2009; Corenblit et al., 2021) by influencing surface microtopography (Reichman and Seabloom, 2002; Kinlaw and Grasmueck, 2012; Debruyn and Conacher, 1994), and soil properties such as soil porosity, permeability and infiltration (Reichman and Seabloom, 2002; Yair, 1995; Hancock and Lowry, 2021; Ridd, 1996; Hall et al., 1999; Coombes, 2016; Larsen et al., 2021). Cumulatively, these modifications lead to changes in sediment redistribution (Gabet et al., 2003; Nkem et al., 2000; Wilkinson et al., 2009) and hence have the potential to affect surface topography and nutrient redistribution on large spatial and temporal scales. To quantify these effects, the shared role of climate, landscape characteristics and burrowing dynamics on sediment redistribution needs to be understood.

On a local scale, currently used field methods to monitor sediment redistribution under real-life condition are mainly erosion pins, splash boards, or rainfall simulators (Imeson and Kwaad, 1976; Wei et al., 2007; Le Hir et al., 2007; Li et al., 2019a; Li et al., 2019b; Li et al., 2018; Voiculescu et al., 2019; Chen et al., 2021; Übernickel et al., 2021a). The monitoring of box experiments yields a high spatio-temporal resolution, and can also be linked with mathematical equations, such as random walks (Boudreau, 1986; Wheatcroft et al., 1990), stochastic differential equations (Boudreau, 1989; Milstead et al., 2007), finite difference mass balancing (Soetaert et al., 1996; François et al., 1997) or Markov chain theory (Jumars et al., 1981; Foster, 1985; Trauth, 1998; Shull, 2001) to describe sediment redistribution.

Previously used methods have, however, several limitations when studying bioturbation. Field measurements likely lead to an underestimation of sediment fluxes, as they are one-time or seasonal measurements, and thus do not capture the continuous excavation of the sediment by the animal (Grigusova et al., 2022) at a high temporal resolution. Box experiments and from them derived mathematical equations describe bioturbation as an isolated process and ignore adjacent environmental parameters (such as climate or vegetation). However, the field measurements showed both, positive (Hazelhoff et al., 1981; Black and Montgomery, 1991; Chen et al., 2021) and negative impact of bioturbation on erosion (Imeson and Kwaad, 1976; Hakonson, 1999). Also, previous field based studies observed an increased bioturbation activity with higher (Milstead et al., 2007; Meserve, 1981; Tews et al., 2004; Wu et al., 2021; Ferro and Barquez, 2009), but also with lower vegetation cover (Simonetti, 1989; Zhang et al., 2020; Zhang et al., 2019; Qin et al., 2021). Furthermore, soil mixing rates are not homogenous throughout the year but depend on the animal phenological cycles (Eccard and Herde, 2013; Jimenez et al., 1992; Katzman et al., 2018; Malizia, 1998; Morgan and Duzant, 2008; Monteverde and Piudo, 2011; Gray et al., 2020; Yu et al., 2017).

Another approach offer raster-based soil erosion and landscape evolution models which integrate co-dependencies between bioturbation relevant environmental parameters (Black and Montgomery, 1991; Meysman et al., 2003; Yoo et al., 2005; Schiffers et al., 2011). Most common soil erosion models are empirical (Wischmeier and Smith, 1978; Williams, 1975; Renard et al., 1991), process-based (Morgan et al., 1998; ROO et al., 1996; Nearing et al., 1989; Beasley et al., 1980), or semi-empirical models, the latter of which are a combination of both (Morgan et al., 1984; Beven and Kirkby, 1979).

Process-based models are based on a mechanistic understanding of the underlying physical, chemical, and biological processes that govern the behaviour of the system being studied. They must be

parametrised for each site; however, these models explicitly represent the governing equations and simulate the system's behaviour by numerically solving these equations. Process-based models are generally considered to be more realistic and accurate than empirical models because they capture the fundamental processes that drive the system's behaviour. However, process-based models can be computationally expensive, require more data and knowledge of system properties, and may require complex numerical algorithms (Morgan et al., 1998; ROO et al., 1996; Nearing et al., 1989; Beasley et al., 1980).

Within empirical models, on the other hand, the physical equations are completely replaced by empirically determined equations which only hold for the specific area they are derived for. These models are generally simpler, less computationally expensive, and require more data and knowledge of system properties than process-based models. However, empirical models also tend to be less accurate than process-based models, particularly when applying beyond the range of data used to fit the model. In contrast to physical-based models, empirical models may not be applicable to new or different conditions, as they are based on observed relationships and do not capture the underlying processes that govern system behaviour (Wischmeier and Smith, 1978; Williams, 1975; Renard et al., 1991).

Semi-empirical models combine the advantages of the both model types (Morgan et al., 1984; Morgan, 2001; Morgan and Duzant, 2008; Devia et al., 2015; Lilhare et al., 2015).

Most landscape models do not yet implement impacts of bioturbators on water and sediment fluxes (Brosens et al., 2020; Anderson et al., 2019; Braun et al., 2016; Cohen et al., 2015; Cohen et al., 2010; Carretier et al., 2014; Welivitiya et al., 2019). There are numerous models describing benthic soil mixing (Francois et al. 1997, Francois et al. 2002, Kadko and Heath 1984, Croix et al. 2002), biodiffusion caused by all invertebrate bioturbators (Maysman et al. 2005, Rakotomalala et al. 2015, Morris et al. 2006) or vertical soil mixing and lateral sediment redistribution caused by single invertebrate species (Orvain et al. 2006, Román – Sánchez et al. 2019, Orvain 2005, Orvain 2003, Sanford 2008). However, there are also models which described the impact of bioturbation on sediment redistribution by the vertebrate animal species: such as the impact of pocket gophers on non-linear hillslope diffusion (Gabet 2000) or on the creation of Mima mounds (Gabet et al. 2014). Several models include soil vertical mixing caused by bioturbation and its effect on landscape evolution on a millennial scale. This rather large spatio-temporal scale however means an omission of the natural variability in burrow sizes and densities, climate zones and seasonality. In these models, soil erosion is proportionally increasing with increasing bioturbation, vertical soil mixing rates are uniform, and bioturbation is positively linked with vegetation cover (Temme and Vanwalleghem, 2016; Vanwalleghem et al., 2013; Yoo and Mudd, 2008; Pelletier et al., 2013). None of the previous studies included vertebrate bioturbator burrows of various sizes and spatial distribution by adjusting the soil properties and topography into a raster-based area-wide soil erosion model. This approach would enable to understand impact of all vertebrate bioturbators by considering the spatial distribution and variable impacts of bioturbator burrows on sediment redistribution. For this, bioturbation has to be included into erosion models at a spatial resolution which allows to imitate the surface processes occurring within and near the burrow, and at a temporal resolution which captures the animal daily burrowing behaviour.

A suitable model which can be extended to include continuous bioturbating activity is the semi-empirical Morgan – Morgan – Finney soil erosion model (Morgan et al., 1984; Morgan, 2001). This model was

successfully tested in several climate zones and land use types, such as Mediterranean sites (Jong et al., 1999), rainfed agrosystems, fields and pastures (López-Vicente et al., 2008), East-African Highlands (Vigiak et al., 2005) or humid forests (Vieira et al., 2014). One of the recently developed improvements of this model is the Daily Morgan – Morgan – Finney model (DMMF), which introduces subsurface flow, vegetation structures (type, size, height, root depth), and enables modelling at a high spatial (0.5 m) and temporal (daily) resolution (Choi et al., 2017). These improvements yield the potential to integrate the bioturbation into the model, as the burrowing activity is not constant and depends on vegetation structure (Tews et al., 2004; Ferro and Barquez, 2009).

In this study, we include vertebrate bioturbator burrows into a semi-empirical soil erosion model (DMMF) at a daily temporal and 0.5 m spatial resolution. For this, we predict the distribution of burrows by applying machine learning techniques in combination with using remotely sensed data as predictors. Then, we adjust soil properties, topography and vegetation properties at predicted burrow locations based on field and laboratory measurements. We validate the model using field sediment fences. We run the model for a time period of 6 years, once with and without burrow adjustments. We estimate the impact of bioturbator burrows on sediment redistribution (including accumulation, erosion, and excavation), and surface runoff within four sites along the Chilean climate gradient. Lastly, we analyse how the impact of bioturbation on sediment redistribution depends on the burrow structure, climate, topography, and adjacent vegetation. Our study shows the importance of including bioturbation into erosion modelling, and describes the interplay between bioturbation, environmental parameters such as… and sediment redistribution.

2. Study area

Our study was performed along a climate and vegetation gradient in Chile (Übernickel et al., 2021b), comprising four study sites in the Chilean Coastal Cordillera: Pan de Azúcar (PdA) National Park (NP), Santa Gracia (SG), La Campana (LC) NP, and Nahuelbuta (NA) NP (Fig. 1). PdA NP is located in the arid zone in a fog-laden environment in the southern part of the Atacama Desert, with almost no rainfall. The vegetation cover is less than 5 % and dominated by small desert shrubs, several types of cacti and biocrusts (Lehnert et al., 2018). SG is a natural reserve located in the semi-arid zone near La Serena, which is dominated by goat grazing. The vegetation consists of shrubs and cacti, covering up to 40 % of the study area. LC NP is part of the Mediterranean-type climate zone in the Valparaiso Region and is also affected by cattle. The study site is dominated by an evergreen sclerophyllous forest with endemic palms. The canopy reaches a height of up to 9 m, and the understory consists of deciduous shrubs and herbs. NA is located in the humid-temperate zone and characterized by a dense evergreen *Araucaria* forest comprising broadleaved trees with heights of up to 14 m. The ground is covered by bamboo, shrubs, and herbs (Bernhard et al., 2018; Oeser et al., 2018). The most common bioturbating vertebrate animal species recorded within these sites are carnivores of the family Canidae (*Lycalopex culpaeus*, *Lycalopex griseus*) as well as rodents of the families Abrocomidae (*Abrocoma bennetti)*, Chnichillidae (*Lagidium viscacia)*, Cricetidae (*Abrothrix andinus, Phyllotis xanthopygus*, *Phyllotis limatus, Phyllotis darwini*) and Octogontidae (Cerqueira, 1985; Jimenez et al., 1992; Übernickel et al., 2021a).

287
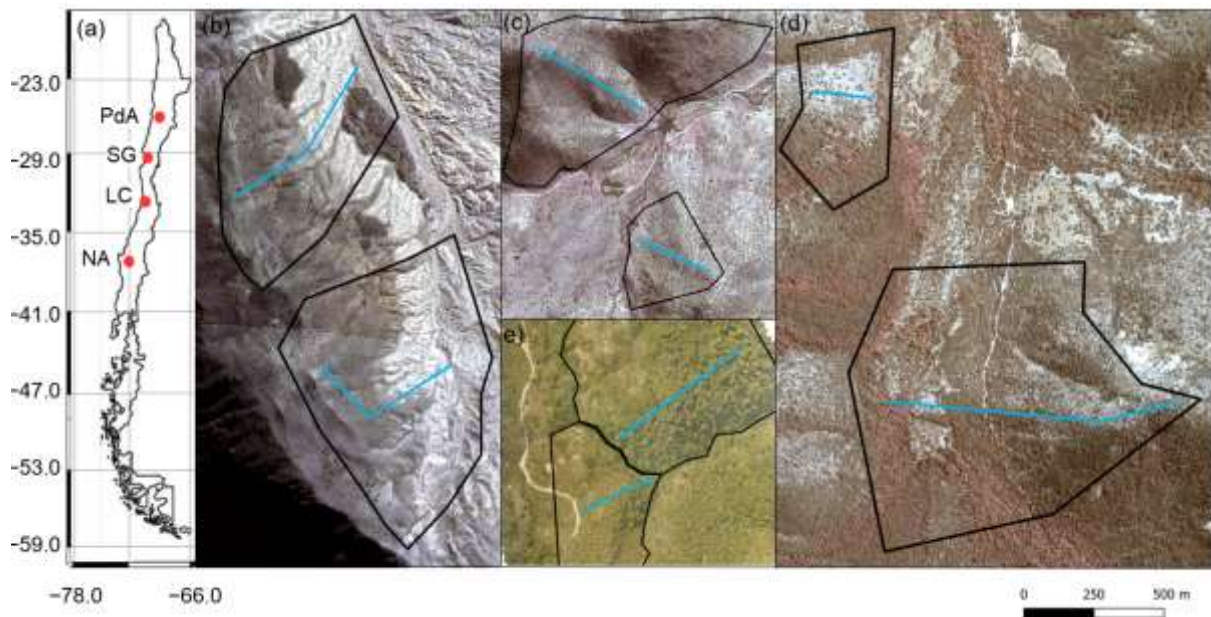
Figure 1. Study area and study sites. Black lines outline the hillslope catchments. Along the blue lines, the in situ data (mound locations, soil samples, vegetation mapping) were collected. (a) Position of the study sites along the climate gradient. PdA = Pan de Azúcar, SG = Santa Gracia, LC = La Campana, NA = Nahuelbuta; Positions of plots in (b) PdA; (c) SG; (d) LC; and (e) NA. The background image is an RGB-composite calculated from WorldView-2 satellite imagery. Images were obtained with single license from GAF AG. Scale bar is the same for (b), (c), (d) and (e).

3. Methodology

We combined semi-empirical soil erosion modelling with in-situ measurements, remote sensing data and machine learning methods (Fig. 2). Along 8 hillslope catchments within 4 climate zones we mapped locations of burrows, estimated the vegetation cover and extracted soil samples. We analyzed the soil samples in the laboratory. Then we used remote sensing datasets and machine learning to upscale burrow distribution, vegetation cover and soil properties into the hillslope catchments. The hillslope catchment-wide predictions, the topographical information retrieved from LiDAR data (Kügler et al., 2022) and the climate information retrieved from climate stations were the input parameters for our soil erosion model. We ran the model with and without bioturbation. We included the bioturbation into the model by adjusting the input parameters at the predicted burrow locations, by including the continuous burrowing activity and soil mixing (Grigusova et al., 2021), and the seasonality (Kraus et al., 2022).and the animal phenological cycle as found in (Jimenez et al., 1992). The models were validated using self-constructed sediment traps. We studied the modeled surface runoff and sediment redistribution. Lastly, we analyzed if and how the impact of bioturbation on sediment redistribution depends on environmental parameters (topography, landscape connectivity and vegetation).

310

311
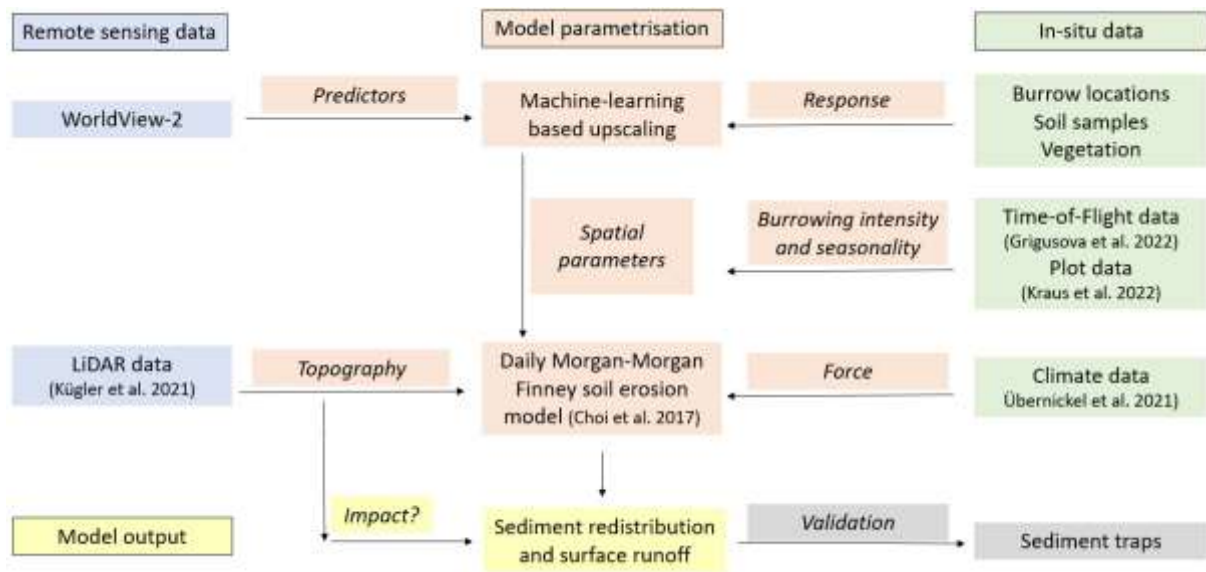
312

313 **Figure 2.** Flow chart of our study. Green color indicates in-situ input data, blue indicates remote sensing

314 input data. Red indicates Model parametrization. Yellow indicates model output and analysis. Grey

315 indicates model validation.

316

317 **3.1 In-situ data**

318 The study set-up consisted of eight hillslope catchments: one north-facing and one south-facing hillslope

319 catchment per study site. We defined a line with a width of one meter from the top to the base of each

320 hillslope catchment (see blue line, Fig. 1). We subdivided the track into tiles of 1 m². We saved the GPS

321 information of each tile.

322 Within each tile of the line, we mapped burrow presence, land cover and extracted soil samples. A

323 burrow consisted of an entrance and a mound (Fig. 3a). Each 1 m² tile with a burrow was described as

324 a presence data point, tiles without a burrow as absence data points. We noted the size of the burrow,

325 vegetation cover and land cover types (bare soil, herbs, shrubs, trees) within the tile. We extracted 162

326 soil samples from soil without a mound at a depth of 10 cm. Additionally, we took a photo of the surface

327 every second tile along the track.

328 To validate the model output, we set up sediment traps (Fig. 3b), with six traps per site, two of which

329 were located at the hillslope catchment base and four were located on two random positions within the

330 hillslope catchment. The sediment traps consisted of geotextile vertically attached to wooden poles for

331 stability. The traps had a length of 2 m – 5 m, a width of ~1.5 m and a height of ~1 m. 1.5 m of geotextile

332 was laid down at the surface uphill the wooden poles to enable the collection of sediment. The sediment

333 accumulated within the traps was collected after 1 year and its mass [cm³] and dry weight [kg] were

334 estimated.

335 Climate information was retrieved from climate stations located adjacent to the hillslope catchments

336 which provide climate data in 5 minute intervals (Übernickel et al. 2021). To force the model on an hourly

337 basis, hourly air temperature, precipitation total and intensity, wind speed, wind direction and humidity

338 was calculated for the study period from 1st April 2016 to 1st December 2021. Evapotranspiration was

339 estimated by the Penman-Monteith equation (Penman, 1948).

340
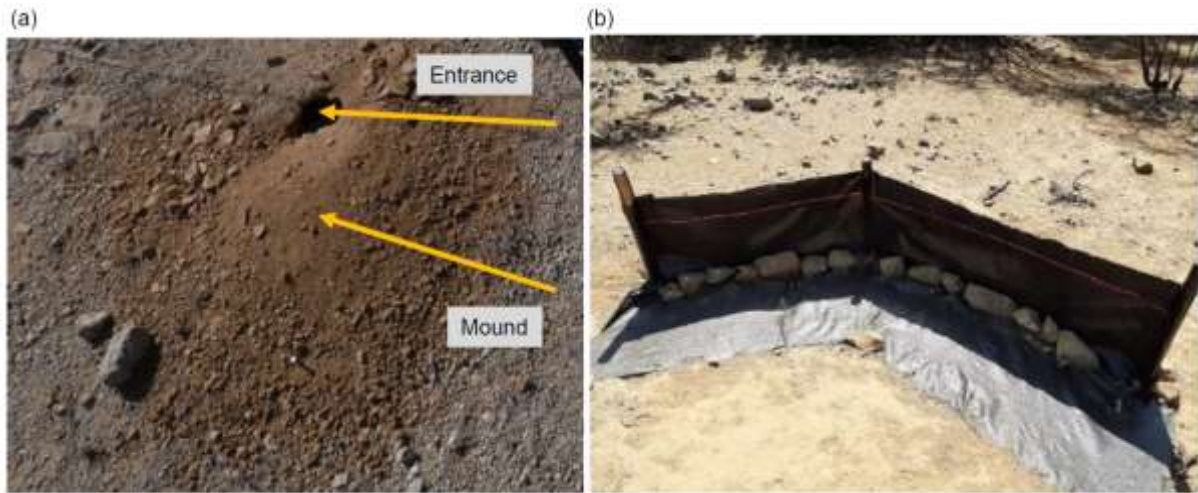
341

342 **Figure 3.** In-situ constructions. (a) Example of a burrow consisting of burrow entrance and mound. (b)
343 Fence construction used for the collection of eroded sediment to validate the model. Both photos by
344 Paulina Grigusova.

345

346 **3.2 Estimation of soil properties**

347 We estimated several soil properties from the soil samples and photos collected in-situ ((Grigusova et
348 al., 2022). We estimated the rock coverage on the surface and debris from the photos taken every
349 second tile. For this, the photos were firstly classified into 5 classes. The classification was unsupervised
350 using k-means (Fig. A1). Then we calculated the ratio of pixels classified as skeleton and / or debris to
351 the overall amount of all pixels to determine the amount of both parameters in percent.

352 In the lab, we estimated soil water content, bulk density, soil particle density, soil texture (sand, silt, clay,
353 coarse / middle / fine sand, coarse / middle / fine silt), soil skeleton, organic matter and organic carbon.
354 Gravimetric soil water content [%] (GSWC) described the mass of water within the soil sample and was
355 estimated as in Eq (1):

356 $$GSWC = \frac{(Sm-Sd)}{Sd} * 100 \quad , \tag{1}$$

357 where Sm [g] is the mass of moist soil measured directly after the extraction and Sd [g] is the mass of
358 soil dried at 105 °C for at least 24 hours. Bulk density [g cm⁻³] (BD) was calculated as following:

359 $$BD = \frac{Sd}{Sv} \quad , \tag{2}$$

360 where Sv [cm³] is the volume of the sample. Soil particle density [g cm⁻³] (SPD) was calculated as in Eq
361 (3):

362 $$SPD = \frac{dm}{Sv} \quad , \quad , \tag{3}$$

363 where dm [g] is the dry mass of soil particles excluding pores.

364 Particle size distribution [%] – clay (< 0.002 mm), coarse, middle and fine silt (0.002 mm to 0.02 mm),
365 and coarse, middle and fine sand (0.02 mm to 2 mm) was estimated using a PARIO method (Durner et
366 al., 2017). Soil skeleton was estimated as the ratio of particles with a diameter above 2 mm. Ratio of
367 organic matter (OM) was estimated as in Eq. (4)

368 $$OM = 1 - \frac{Sc}{Sd} \quad , \tag{4}$$

369 where Sc is the weight [g] of the sample dried at 500 °C for 16 hours.

370 We used pedotransfer functions to determine porosity, saturated soil moisture, hydraulic conductivity,

371 water content at field capacity, and permanent wilting point. Pore ratio (θs) was estimated from bulk and

372 particle density as in Eq. (5):

373 $\theta s = \frac{BD}{SPD}$ (5)

374 Saturated water content [g g^{-1}] (Ws) was estimated as in Eq. (6):

375 $Ws = \theta s \frac{pw}{BD}$, (6)

376 where pw [g cm^{-3}] is the density of water which is set to be 1 g cm^{-3} (Pollacco, 2008).

377 Hydraulic conductivity Ks [m s^{-1}] was estimated as in Eq. (8):

378 $Ks = 1.15741 * 0.0000001 * \exp(x)$, (7)

379 where x for sandy soil is:

380 $x = 9.5 - 1.471 * (BD * BD) - 0.688 * OM + 0.0369 * (OM * OM) - 0.332 * CS$, (8)

381 and x for loamy and clayey soils is:

382 $x = -43.1 + 64.8 * BD - 22.21 * (BD * BD) + 7.02 * OM - 0.1562 * (OM * OM) + 0.985 * \ln(OM) -$

383 $0.01332 * C * OM - 4.71 * BD * CS$, (9)

384 where C is percentage of clay and CS is percentage of clay and silt (Wösten, 1997). To estimate water

385 content at field capacity [%] (FC) and permanent wilting point (PWP), we applied functions by (Tomasella

386 et al., 2000) as these were developed for South American soils:

387 $FC = 4.046 + 0.426 * Si + 0.404 * C$, (10)

388 $PWP = 0.91 + 0.15 * Si + 0.396 * C$, (11)

389 where Si is the percentage of silt.

390

391 **3.3 Processing of remote sensing data**

392 The digital elevation models (DEM) were calculated from the LiDAR data (Kügler et al., 2022; Horn,

393 1981) at a resolution of 0.5 m. Slope was calculated according to Horn (1981). Manning's surface

394 roughness coefficient was estimated following (Li and Zhang, 2001). Topographic position index (TPI)

395 and Topographic ruggedness index (TRI) were calculated according to (Wilson et al., 2007). TPI subtract

396 the mean elevation of pixels in a specified range from the elevation of the central pixel. Positive values

397 represent hills while negative values represent valleys. The TRI adds together the elevation differences

398 between a grid cell and its eight neighbours. It measures the relative level of topography irregularity, the

399 higher the value, the more irregular the topography. Plan and profile curvature were determined after

400 (Zevenbergen and Thorne, 1987). Connectivity indices, Sinks, Wetness index, Flow direction, Flow path,

401 Catchment slope and Catchment were calculated in SAGA GIS.

402 Single license stereo WorldView-2 images with a resolution of 0.5 m were retrieved from GAF Munich

403 GmbH. The topographic correction of WorldView-2 images was done using the LiDAR data, solar

404 elevation angle, solar zenith angle and azimuth angle according to Goslee (2019). The digital surface

405 models (DSMs) were calculated from the stereo images. Additionally, we extracted single bands and

406 calculated the normalized difference vegetation index (NDVI).

407

408 **3.4 The erosion model**

409 **3.4.1 Daily Morgan-Morgan-Finney model**

410   The DMMF model is a combined soil erosion model used to estimate surface runoff and sediment flux
411   on a field scale on a daily basis. Spatially, the DMMF model represents an area as several
412   interconnected elements (e.g. pixels) of uniform topography, soil characteristics, land cover type, and
413   vegetation structure. Through coupling, the model operates with flow direction algorithms: each element
414   receives water and sediments from upslope elements and delivers the generated surface runoff and
415   eroded soils to downslope elements. On a temporal scale, the model estimates surface runoff and
416   sediment flux of each element on a daily basis. The model input parameters include climate, topography,
417   soil properties and land cover information (Choi et al., 2017). Data pre-processing, modelling and
418   analysis (see Fig. 2) was done in R statistic environment. The raster data were cropped to the size of
419   the hillslope catchments (Fig. 1). Input parameters are listed in Table 1 and plotted in Fig. A2.

420   During the model simulation, water and sediment are transferred from pixels located at higher elevations
421   to pixels situated at lower elevations. This occurs in two stages: The first stage is the hydrological phase
422   where the model calculates surface runoff which happens when the amount of surface water input
423   exceeds the water-holding capacity. The amount of surface runoff is computed by taking the infiltration
424   capacity of the surface, the volume of surface water input, and the fraction of the impervious area of a
425   pixel into account. Infiltration capacity represents the maximum amount of surface water that can
426   penetrate the subsurface layer. It is determined by the percentage of the impervious area and the
427   available pore space.

428   The second stage is the sediment phase, where the model estimates the sediment budget for each
429   particle size class, based on the surface conditions. The model calculates the detachment and
430   deposition of sediments in a step-by-step process. The sources of sediments are detached particles
431   from the pixel itself due to rainfall and surface runoff, and delivered soil particles from higher elevation
432   pixels. The detachment of soil particles by rainfall occurs when raindrops hit the ground with enough
433   energy to detach soil particles from the surface. Rainfall has different impacts on areas with and without
434   canopy cover, as canopy cover changes the kinetic energy of raindrops.

435   The amount of soil particles detached by raindrops is calculated based on the soil particle detachability,
436   the percentage of each particle size class, the bare soil surface area, and the kinetic energy of effective
437   rainfall. The amount of detached soil particles by surface runoff is calculated based on the soil particle
438   detachability, the amount of runoff, the slope angle of the pixel, and the proportion of the bare surface
439   area. The third source of sediment is from higher elevation pixels and is averaged by the surface area
440   of the pixel.

441   Once sediments are delivered to the surface runoff, a portion of the suspended sediments settles to the
442   bottom due to gravitational force. To calculate this settling, the model requires the flow velocity of the
443   runoff and the settling velocity of each particle size class, which are influenced by the flow depth, slope
444   angle of the pixel, and Manning's roughness coefficient (Choi et ail. 2019).

445

446   **3.4.2 Estimation of spatial parameters**

447   For spatial parameterization of the DMMF model, we predicted land cover, soil properties and burrow
448   distribution onto the hillslope catchments using machine learning techniques.

449   We used the approach Meyer et al. 2018. The most important predictors were selected by forward
450   feature selection. The quality of the random forest models was assessed by Leave-Location-Out cross

validation. We trained the model stepwise, using in-situ data collected from seven of the hillslope catchments and validated the model using in-situ data from the remaining hillslope catchment (Meyer et al., 2018). The prediction was done at 0.5 m spatial resolution. We used the WorldView-2 layers obtained with a single license from GAF, NDVI, DEM, DSM, slope and roughness as predictors. The PAN-sharpening of the WV-2 layers was done by GAF.

For the area-wide prediction of burrow locations across the hillslope catchments, we used the burrow presence and absence data (section 3.1) as the response data within the RF models. The accuracy was 0.82 for PdA, 0.77 for SG, 0.75 for LC and 0.85 for NA. The prediction of soil properties was done using soil properties estimated along the track line (see section 3.1) as response data within the RF models. All of the models reached a high accuracy (see Table A1).

To obtain land cover classification, we used as the response within the RF models the land cover measured in-situ. The classes were soil without rocks, rocks, biocrusts, grass/herbs, shrubs and trees. Predictor values for each class were extracted from at least 100 polygons per site and class. The accuracy of the RF models was 0.71 for PdA, 0.81 for SG, 0.83 for LC and 0.75 for NA.

The vegetation height measured in plots was averaged for each class per site. All pixels classified as respective class were assigned the same vegetation height information. Vegetation density was estimated per hillslope catchment as the amount of vegetation individuals per m^2. Vegetation diversity was calculated by Shannon index (Shannon, 1948). The interception area was the area not covered by vegetation (herbs, shrubs or trees).

3.4.3 Inclusion of bioturbation

In the grid cells with predicted burrow locations, we adapted the values of input parameters to include bioturbation. The adaptations varied with climate zone and burrow size. The size, geometric structure and excavation rates of burrowing animalswere previously estimated at a high spatial and temporal resolution (Grigusova et al., 2022). Based on this results, we firstly adjusted the microtopography. We modified the layer depth to represent burrow entrance and elevation to represent animal mound. Mounds were always located downslope of burrow entrances in the direction of flow.

Secondly, we adjusted the soil properties. Soil properties texture and organic carbon were estimated from soil extracted from mounds in Kraus et al. (2022). In this study we additionally estimated bulk density, initial water content, soil skeleton, porosity, saturated water content, available water capacity and water content at field capacity from the same dataset (see section 3.2). We calculated the median value of each property for the samples extracted from mounds and for the samples extracted from soil without mounds. Then, we estimated the change in percent between these two values. This was then used to adjust the soil property for each pixel including a mound.

Thirdly, modelled mound pixels had to be cleared from ground vegetation cover. For this, we removed ground vegetation cover from pixels with burrow locations and decreased ground vegetation cover, height, diameter and amount of ground vegetation individuals from adjacent pixels as measured in situ. Then, the amount of rocks and debris was set as estimated from soil samples (section 3.2)

Animal activity has been found to be highly variable throughout the year (Grigusova et al., 2022; Kraus et al., 2022). The density of burrows does not stay stable throughout the year but increases or decreases

depending on the season and climate zone. We therefore artificially removed or added burrows into the hillslope catchments at the particular seasons. For this, we adapted the density of soil, the topography and vegetation cover accordingly. We created a 3D-model of the burrow structure, adjusted subsurface soil properties and properties of soil excavated to the surface; the removed vegetation within the pixel with a predicted burrow and decreased adjacent vegetation cover. Animal burrowing activity varies throughout the course of the year, and there is a three-month period during which they are mostly active, which we considered using/doing xxx

Lastly, we also included the vertical movement of sediment particles from deeper soil layers to the surface in dependence on climate. Animals were found to reconstruct their burrows after each rainfall event (Grigusova et al., 2022). Corresponding with these findings, we increased the entrance depth and mound height by 30% after each rainfall event, which represents the averaged value found in the previous study (Grigusova et al., 2022).

For the validation, we ran the model for the time periods between the installation of sediment fences and the collections of sediment. We compared the mass and weight of modelled and collected sediment and estimated R^2 and RMSE. To test the importance of the inclusion of individual bioturbation parameters into the model, we ran the model under 4 conditions: (i) No burrows; (ii) Solely entrances; (iii) Solely mounds; (iv) Entire burrows (entrances and mounds).

Table 1. Model input layers and respective changes to layer values at the predicted burrow locations. Ground vegetation was removed from the respective pixels, while tree canopy was not changed. The values were estimated as described in 3.5.2. Using the adjusted values, we calculated evapotranspiration using the Penman-Monteith equation, surface roughness from the elevation layer, and hydraulic conductivity, water content at field capacity and saturated water content using pedotransfer functions.

Derivation	Parameter	Units	Pixel value at burrow locations			
			PdA	SG	LC	NA
DEM	Elevation	m asl	+0.24	+0.23	+0.36	+0.19
	Surface roughness	-	-	-	-	-
	Depth	m	-0.23	-0.41	-0.22	-0.04
Soil samples	Water content	%	+120	-6	-68	-62
	Bulk density	g cm^{-3}	-	-6	-17	-
	Sand	%	-29	-12	+57	-43
	Silt	%	+54	+22	+23	ns
	Clay	%	+145	+44	+19	-73
	Organic carbon	%	+168	+72	+105	+25
Pedotransfer functions	Hydraulic conductivity	m s^{-1}	-	-	-	-
	Water content at field capacity	%	-	-	-	-
	Saturated water content	%	-	-	-	-
	Ground vegetation cover	%	0	0	0	0

Land cover classification	Soil and debris	%	100	100	100	100
	Skeleton	%	0	0	0	0
	Average plant height	m	0	0	0	0
	Average plant diameter	m	0	0	0	0
	Number of plants	n m^{-2}	0	0	0	0

3.5 DMMF model sensitivity test

We conducted a sensitivity test to identify those input parameters which significantly influence the model output. For this, we first estimated the mean value of each input parameter. Then, we created an artificial hillslope catchment of 100 m * 100 m. To start the test, each pixel received the mean value of each parameter. We ran the model for one rainfall event. Then, we stepwise changed the single input parameter values from their minimum to their maximum values while we did not adjust any other parameters. To quantify the significance of the input variations, we conducted a t-test (Table A2). For this, we compared the amount of redistributed sediment of each model run to the first model run.

3.6 Impact of burrows on surface processes

We estimated burrow density, as a ratio of pixels with predicted burrows to all pixels. Additionally, we calculated the ratio of pixels which are part of a burrow aggregation to all pixels which include a burrow. Burrow aggregation describes at least 4 neighboring pixels with predicted burrows. We calculated the amount of excavated sediment as a sum of burrow density and the burrow excavation rate as estimated in Grigusova et al. (2022).

To estimate the impact of burrows on sediment redistribution and surface runoff, we ran the DMMF model for the time period from 1st April 2016 until 31th December 2021 for all hillslope catchments. We ran the model (i) with no burrows and (ii) with entire burrows. We estimated (i) sediment redistribution (accumulation - erosion) and (ii) surface runoff. We analyzed the redistribution and runoff on the plot (1 m^2) and hillslope catchment (1 ha) scale.

Lastly, to analyze under which biotic and abiotic environmental parameters (topography, vegetation cover) the bioturbation enhances sediment erosion or accumulation, we set-up a generalized additive model (GAM) (Wood, 2006). For this, we first subtracted the output of the model with no burrows from the output of the model with entire burrows. Within each pixel, two processes are happening simultaneously: a certain amount of sediment erodes, and a certain amount of sediment accumulates. To estimate the sediment redistribution for each pixel of each model run, we estimate which of these processes dominated. Positive pixel values thus mean, bioturbation enhanced sediment accumulation, negative pixel values mean, bioturbation enhanced sediment erosion. We tested the following environmental parameters: mound density, vegetation cover, elevation, slope, aspect, TRI, TPI, curvature and connectivity and wetness index. The model performance was evaluated by the percentage of explained data variance. We analyzed the impact of environmental parameters within 1-meter and within 10-meter distance from the burrows.

4 Results

4.1 Model sensitivity test and accuracy

552   Parameters which significantly influenced the model output were precipitation, slope, vegetation cover,

553   surface roughness, silt content and water content (Table A2). There was correlation between some of

554   the spatial model parameters (Fig. A10), especially between the initial and saturated water content;

555   between water content and vegetation cover; and between clay content and field capacity. However, a

556   high correlation between spatial parameters does not mean that these parameters impact the sediment

557   redistribution in a similar way.

558   We quantified the model performance by comparing the modelled and measured sediment

559   redistribution. The performance varied depending on the burrow inclusion (Figure 4 and 5). The

560   performance of the model without any bioturbation was lower (R^2 = 0.73, RMSE = 1.50, MSE = 2.27),

561   as when burrow entrances (R^2 = 0.81, RMSE = 1.34, MSE = 1.16) or mounds (R^2 = 0.83, RMSE = 1.10,

562   MSE = 1.22) were included. The model had the highest performance when entire burrows were included

563   (R^2 = 0.85, RMSE = 1.01, MSE = 1.01). However, as the scatterplots showed, the model performance

564   seemed to be determined strongly by one measurement (Fig. 5). For this reason, we calculated the

565   metrics without this measurement (Fig. A2). The model without any burrows (R^2 = 0.17, RMSE = 1.18,

566   MSE = 1.39) in this case performed much lower than models with burrows. The model performance

567   continuously strongly increased when burrow entrances (R^2 = 0.48, RMSE = 0.61, MSE = 0.78), or

568   mounds (R^2 = 0.51, RMSE = 0.75, MSE = 0.57) were included. The model with whole burrows reached

569   the highest performance (R^2 = 0.71, RMSE = 0.63, MSE = 0.39). When we compare the modelled

570   redistribution to the sediment redistribution estimated using Time-of-Flight cameras in Grigusova et al.

571   (2022), the differences appear to be minor (R^2 = 0.62, RMSE = 0.12, MSE = 0.35).

572
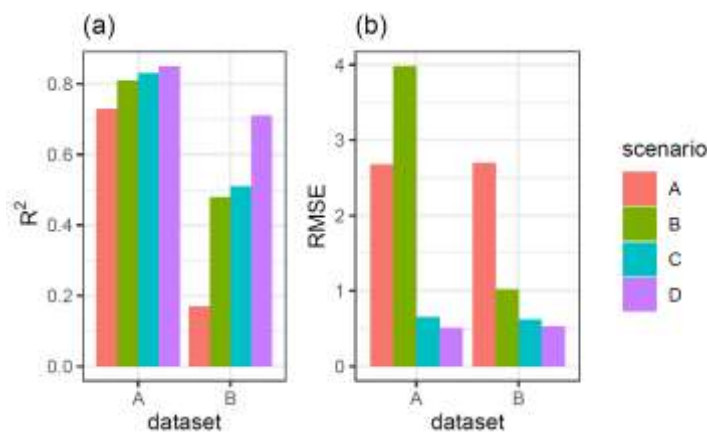
573

574   **Figure 4.** R^2 and RMSE of the Morgan-Morgan-Finney soil erosion model. For dataset A, we compared

575   the amount of sediment collected in all sediment fences with the modelled eroded sediment (see Fig.

576   A3). For dataset B, we removed one measurement, as the R^2 seemed to be defined by this

577   measurement (see Fig. A4). For Scenario A, we did not include any burrows into the model. For scenario

578   B, we included burrow entrances and for scenario C, we included mounds. For scenario D, we included

579   whole burrows into the model. The adjustments made to include entrances, mounds and burrows into

580   the model are described in section 3.5.2.

581
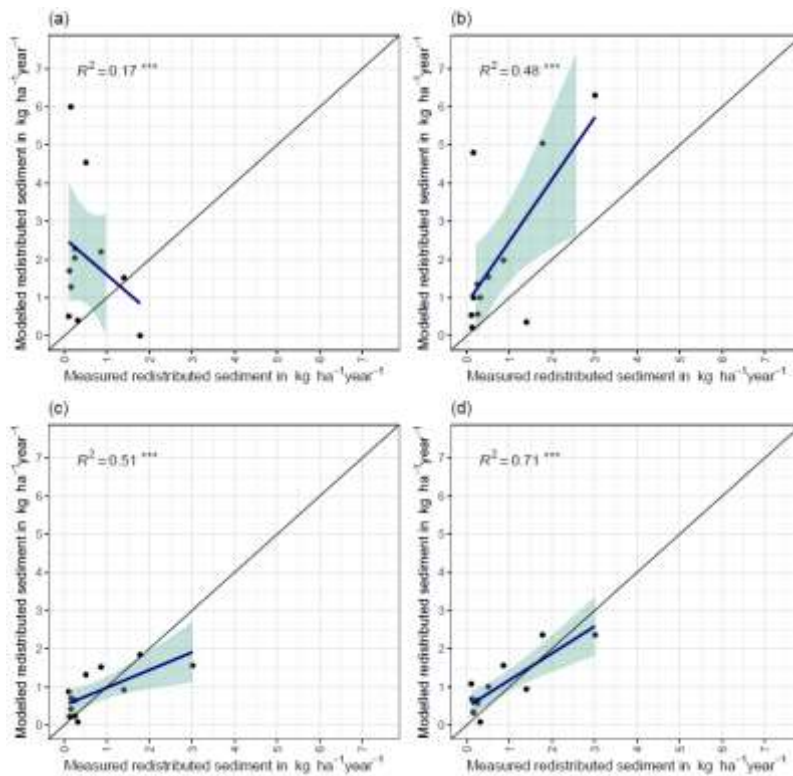
582
583

584 **Figure 5.** Measured and modelled redistributed sediment without an outlier. (a) Model without
585 bioturbation. (b) Model with entrances. (c) Model with mounds. (d) model with burrows.

586

587 **4.2 Model output: Surface runoff and sediment redistribution**
588 Hillslope catchment – wide sediment redistribution (1 ha resolution) was the highest in humid NA,
589 followed by Mediterranean LC, semi-arid SG and arid PdA (Fig. 6a, 6b, 8). In NA, LC and SG, the erosion
590 processes dominated, while in PdA, more sediment accumulated than eroded. The impact of burrows
591 on sediment redistribution was significant in arid PdA, semi-arid SG and Mediterranean LC. Burrows
592 increased sediment redistribution by 137.8 % ±16.4 % in arid PdA (3.53 kg ha^{-1} year^{-1} vs. 48.79 kg ha^{-1}
593 year^{-1}), by 6.5 % ±0.7 % in semi-arid SG (129.16 kg ha^{-1} year^{-1} vs. 122.05 kg ha^{-1} year^{-1}) and by 15.6 %
594 ±0.3 % in Mediterranean LC (4602.69 kg ha^{-1} year^{-1} vs. 3980.96 kg ha^{-1} year^{-1}). Overall, bioturbation
595 increased sediment accumulation in the arid zone (as the magnitude of the sediment excavation by the
596 animal exceeded sediment erosion which occurs during rainfall events), but increased sediment erosion
597 in semi-arid and Mediterranean climate (where animal burrowing activity and rainfall is present). The
598 largest impact was found under Mediterranean conditions. We found no significant effect on
599 redistribution in the humid zone (Figure 7). However, impact of bioturbation varied throughout the
600 hillslope catchment (Figure 7, 8 and 9) – it depended on a specific context if bioturbation supports
601 sediment erosion or accumulation.
602 Surface runoff was the highest in humid NA, followed by Mediterranean LC, arid PdA and semi-arid SG
603 (Figure 6c). The impact of burrows on surface runoff was significant in all climate zones. Burrows
604 increased surface runoff in PdA by 34 %, in SG by 40% and in LC by 4.1 %; and decreased surface
605 runoff by 5.9 % in NA. Hillslope catchment-wide maps are shown in Fig. A6-A8.

606
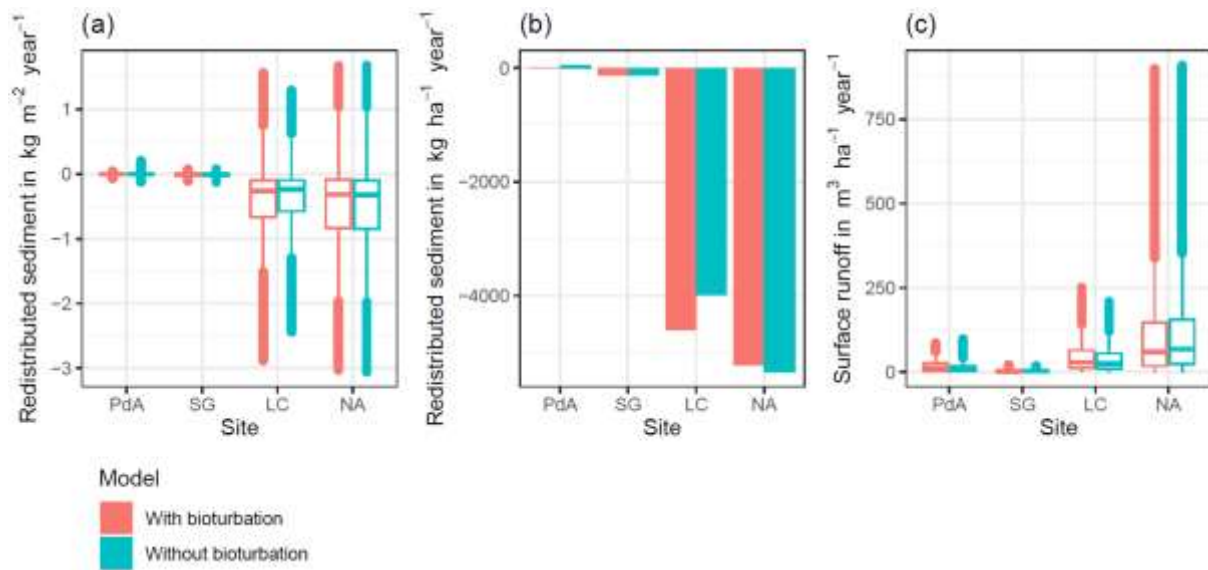
Figure 6. Summary of model outputs across the climate gradient. PdA is arid Pan de Azúcar, SG is semi-arid Santa Gracia, LC is Mediterranean La Campana, NA is humid Nahuelbuta. Graphs (a) and (b) show the modelled sediment redistribution. Positive values indicate sediment accumulation; negative values indicate sediment erosion, in(a) sediment redistribution is shown on a pixel scale in kg m^{-2} year^{-1}, while in(b) sediment redistribution is shown on the hillslope catchment scale in kg ha^{-1} year^{-1}. The impact of bioturbation on sediment redistribution was estimated by a t-test and was significant in three sites: PdA***, SG** and LC***. Bioturbation increased sediment redistribution by 137.8 % in PdA, by 6.5 % in SG and by 15.6 % in LC. For hillslope catchment-wide maps see Fig. A6-A8. Graph (c) represents the modelled surface runoff on the hillslope catchment scale in m^3 ha^{-1} year^{-1}. The impact of bioturbation on surface runoff was estimated by a t-test and was significant at all sites. Bioturbation increased surface runoff in PdA by 34 %, in SG by 40 % and in LC by 4.1 %; and decreased surface runoff by 5.9 % in NA. For hillslope catchment-wide maps see Fig. A6.
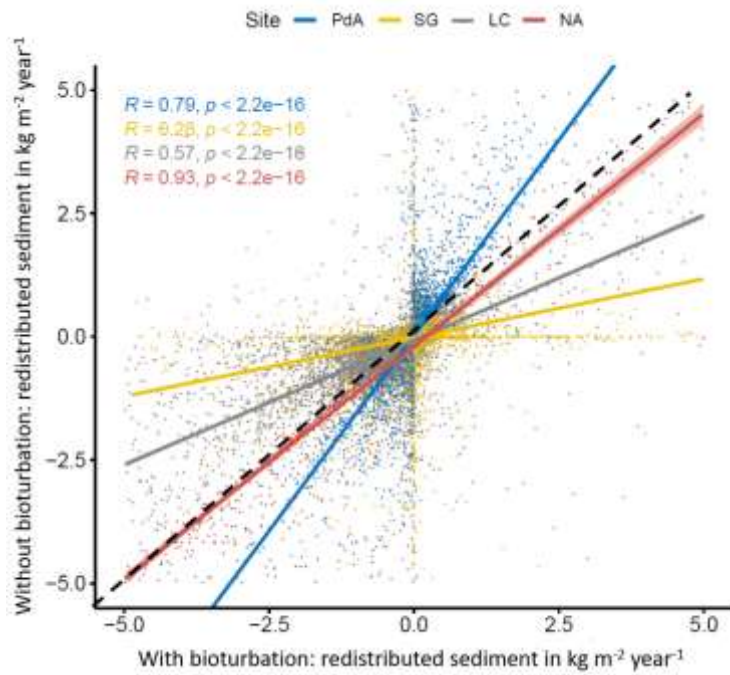
Figure 7. Comparison of the model outputs with and without bioturbation of each pixel (0.5 m) in all study sites. The x-axis shows the output of the model with bioturbation, the y-axis the model output without bioturbation. PdA is arid Pan de Azúcar, SG is semi-arid Santa Gracia, LC is Mediterranean La Campana, NA is humid Nahuelbuta. Points represent single pixel values; lines show linear regressions for the sites. The lower R, the higher the impact of burrows on sediment redistribution at the resolution of 0.5 m. The black dashed line symbolizes a perfect correlation – along this line the bioturbation would have no effect on sediment redistribution. Bioturbation lead to more accumulation if the regression line representing results from a particular climate zone is steeper than the perfect correlation line. Bioturbation lead to more erosion if the regression line representing results from a particular climate zone is flatter than the perfect correlation line. Bioturbation increases sediment accumulation in arid PdA (through the high burrowing rate, more sediment is accumulated on the surface than eroded during rainfall events). Bioturbation increases sediment erosion in semi-arid SG and Mediterranean LC. Absolutely, the highest impact on sediment redistribution is in the Mediterranean climate zone. The lowest impact is in the humid zone.
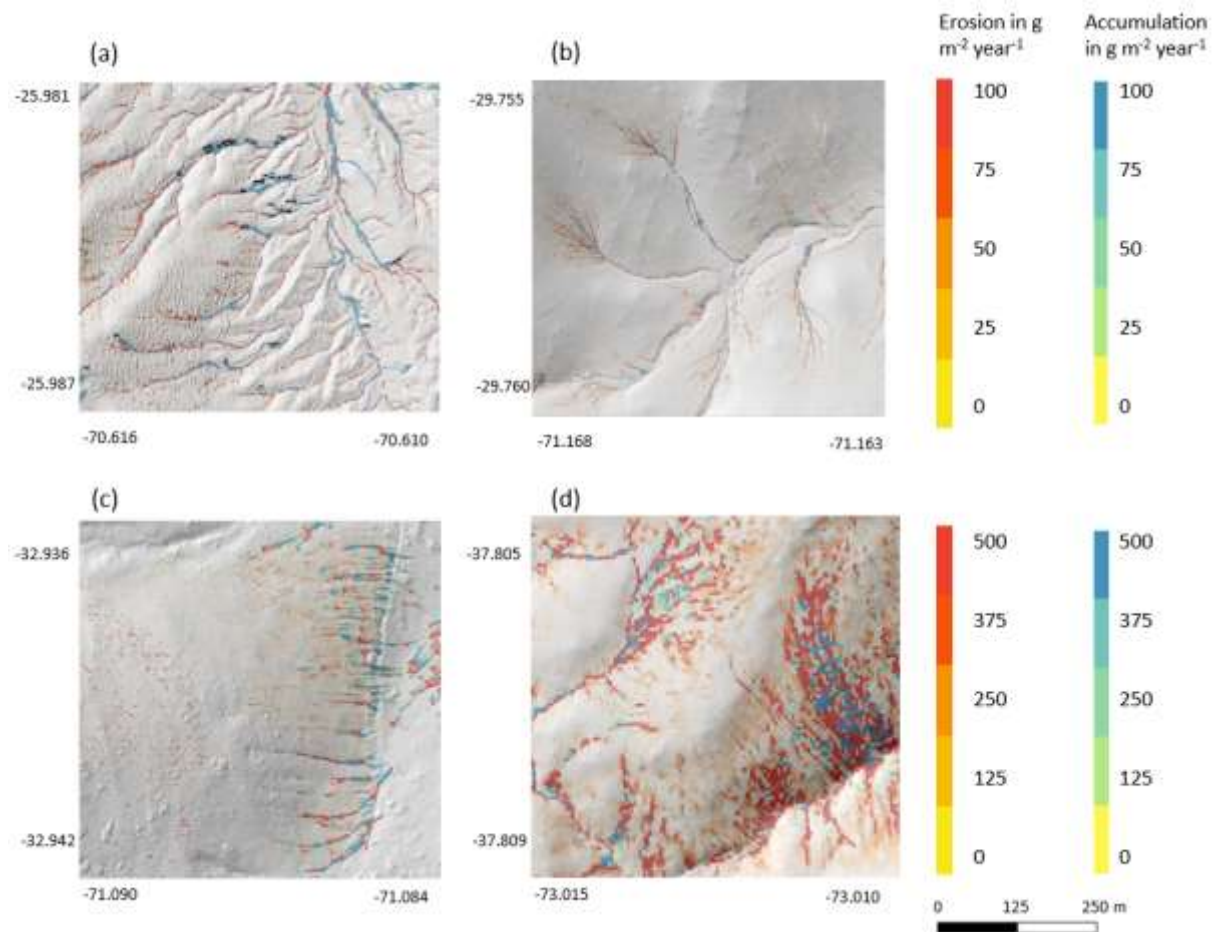
Figure 8. Hillslope catchment-wide predicted sediment redistribution. Colours indicate sediment redistribution. Grey shadows indicate the hill shading calculated from LiDAR data. (a) Pan de Azúcar, (b) Santa Gracia, (c) La Campana, (d) Nahuelbuta.

4.3 Role of continuous burrowing activity on sediment redistribution

We included the excavation of the sediment by the animal itself into the model. The density of burrows was the highest in arid PdA, then Mediterranean LC, semi-arid SG and the lowest in humid NA. Burrows were mostly distributed within groups of several burrows in Mediterranean LC and semi-arid SG, while they were more evenly distributed in arid PdA and humid NA. The burrows were of largest size in Mediterranean LC, followed by arid PdA, semi-arid SG and humid NA. Similarly, the highest volume of excavated sediment at the beginning of the modelling period was in Mediterranean LC and arid PdA. The volume of excavated sediment during the burrow reconstruction after rainfall events was the highest in humid NA, followed by Mediterranean LC, semi-arid SG and arid PdA. The percentage of sediment excavated by the animal to sediment redistributed during rainfall events was 128 % in PdA, 24 % in SG, 33.5 % in LC and 5.6 % in NA.

Table 2. Impact of animal bioturbation activity on overall sediment redistribution on various scales. The bioturbation activity was estimated using Time-of-Flight based cameras in Grigusova et al. 2022. This study showed that animals reconstruct their burrows after each rainfall events. During this process, 10 % of the overall sediment burrow volume is relocated from within the burrow to the surface. We

659 integrated this process into our model and calculated the percentage of newly excavated sediment by

660 the animals to the amount of sediment which was redistributed during rainfalls for the period of one year.

Parameter	Units	PdA	SG	LC	NA
Burrow density	ha^{-1}	91.35	71.50	84.36	13.30
Burrow aggregations	%	24	62	73	5
Burrow size	m^3	0.015	0.012	0.047	0.008
Sediment at the surface at the start of modelling	m^3 ha^{-1}	1.35	0.88	4.11	0.10
Sediment excavated after each rainfall	m^3 ha^{-1}	0.07	0.04	0.22	0.01
Number of rainfall events	year^{-1}	3	7	16	137
Sediment excavated by the animal after the rain	m^3 ha^{-1} year^{-1}	0.21	0.28	3.52	0.69
Sediment redistributed due to rainfall	m^3 ha^{-1} year^{-1}	0.44	1.17	10.51	12.21
Excavated sediment to redistributed sediment	%	47	24	33.5	5.6

661

662 **4.4 Role of adjacent environment**

663 We subtracted the output of the model with included burrows from the output of the model without

664 burrows (Figure A8). Although, the burrows on average enhanced sediment erosion on the hillslope

665 catchment – scale, the high–resolution maps unveiled that burrows enhance sediment erosion within

666 some pixels while they rather increased sediment accumulation within others.

667 The amount of data variance explained by the GAM models (see section 3.6.) differed between models

668 (Table A3). Models estimating the impact of environmental parameters on sediment redistribution within

669 1-meter distance from the burrows, explained 3.84 % of variance in PdA, 37.1 % in SG, 46 % in LC and

670 42. % in NA. Models estimating the impact of environmental parameters on sediment redistribution

671 within 10-meter distance from the burrows, explained 1.99 % of variance in PdA, 12.8 % in SG, 52 % in

672 LC and 72.9 % in NA. The parameters selected for SG were slope, roughness, curvature, TRI and NDVI.

673 Parameters selected for LC were elevation, slope, NDVI, sinks and roughness. Parameters selected for

674 NA were elevation, slope, aspect, TRI, sinks and roughness (Figure 10).

675 Bioturbation strongly increased sediment redistribution (erosion and accumulation) at high values of

676 elevation, slope, surface roughness TRI, sinks and topographic wetness index, at the middle values of

677 elevation and aspect, and at low values of profile curvature and NDVI. From these parameters,

678 bioturbation increased sediment erosion at high and middle values of elevation, at high values of slope,

679 sinks and TRI, and at low values of profile curvature. Bioturbation increased sediment accumulation at

680 high values of surface roughness and topographic wetness index and at low values of NDVI (Fig. A3 –

681 A8).

682 Bioturbation somewhat enhanced sediment erosion at medium values of surface roughness, NDVI and

683 sinks, and at low values of topographic wetness index. Bioturbation somewhat increased sediment

684 accumulation at low values of slope and TRI, at low and medium values of elevation and at high values

685 of profile curvature.

686
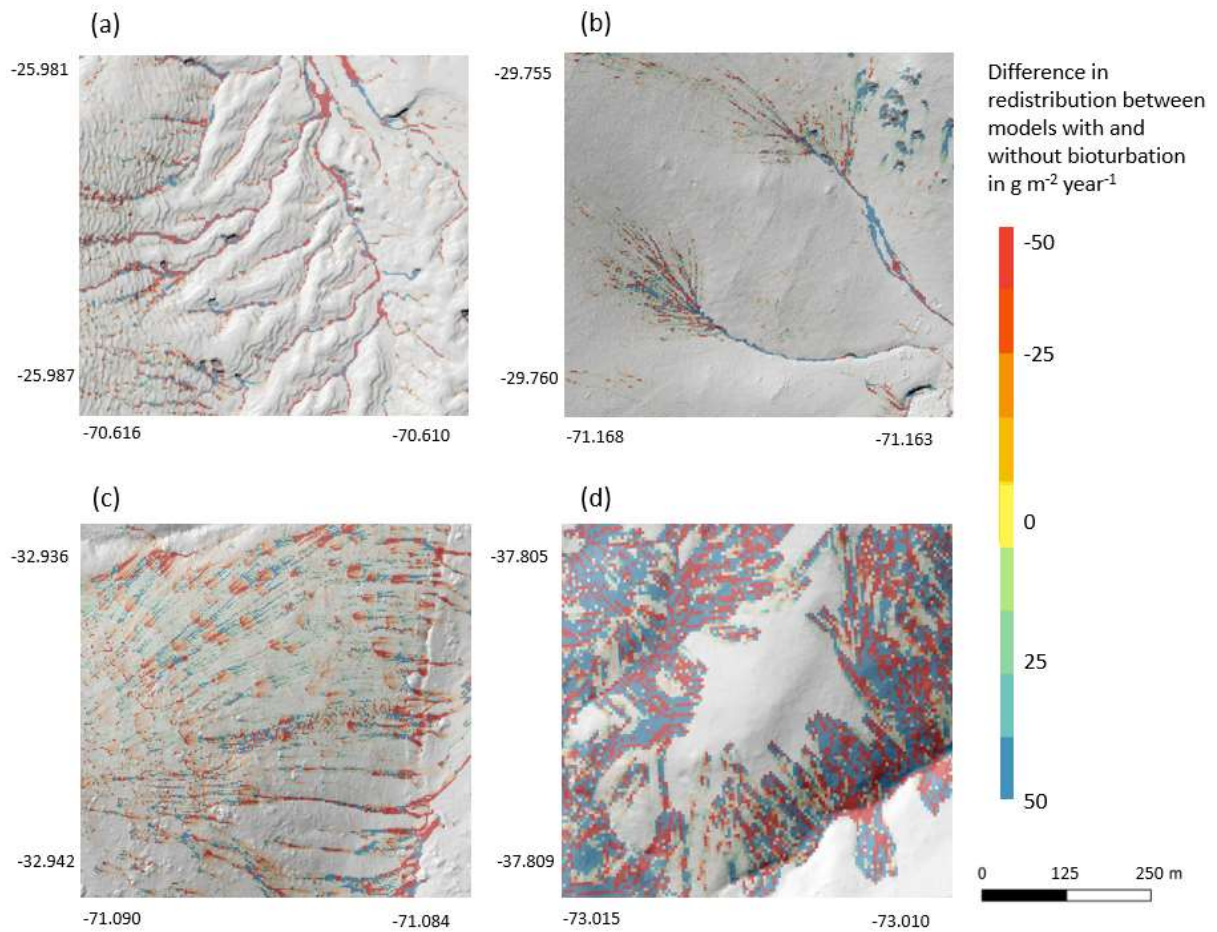
Figure 9. Hillslope catchment-wide impact of bioturbation on sediment redistribution. Colour indicates the impact. Positive values indicate bioturbation enhanced sediment accumulation, negative values indicate bioturbation enhanced sediment erosion. Grey shadows indicate the hill shading calculated from LiDAR data. (a) Pan de Azúcar, (b) Santa Gracia, (c) La Campana, (d) Nahuelbuta.
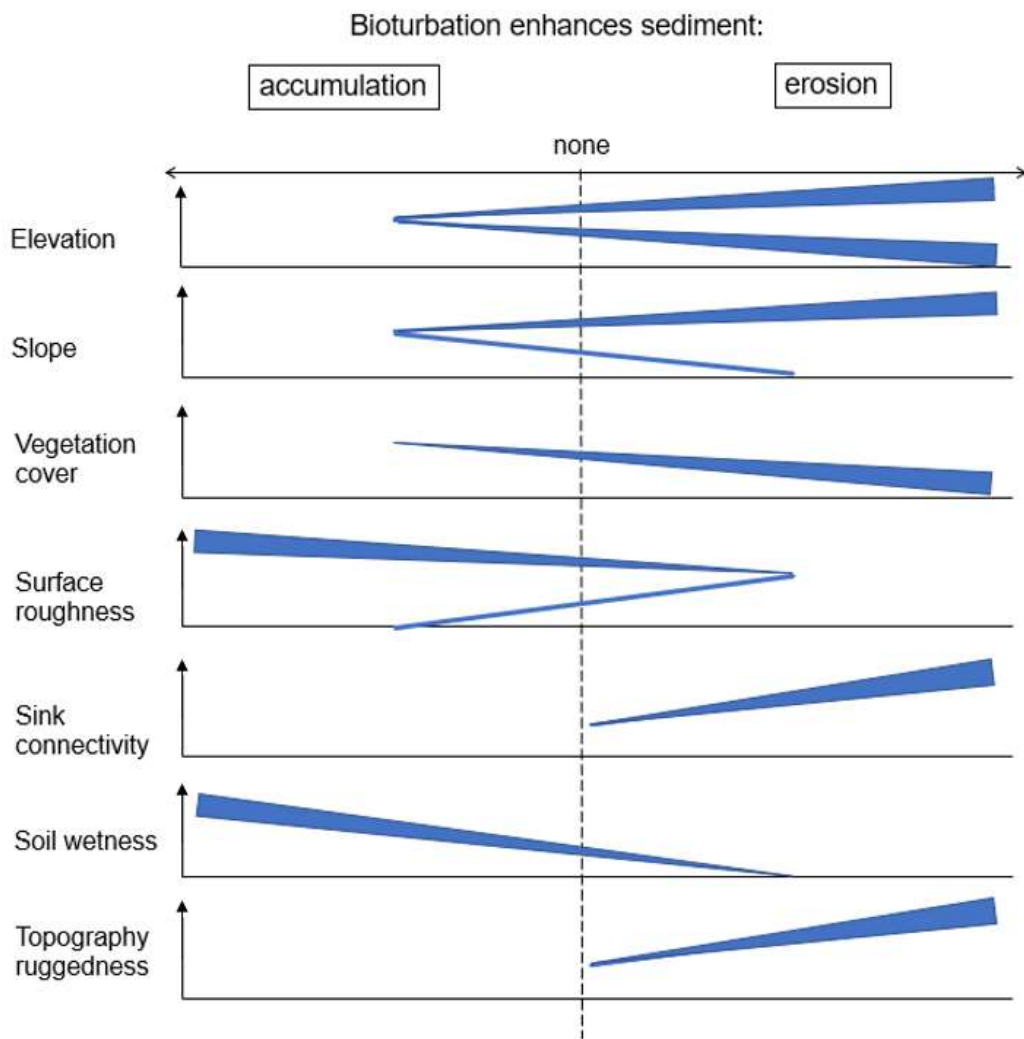
694 **Figure 10.** This figure is a conceptual summary of the detailed results from figures A3 – A8. Bioturbation
695 increases erosion or accumulation depending on the values of environmental parameters. The
696 dependencies are the same for all climate zones. The figure is the conceptual summary for all climate
697 zones, therefore, there are no values stated on the x- and y-axes. The x-axis shows if bioturbation
698 increases erosion or accumulation. The y-axis are environmental parameters. Line thicknesses indicate
699 the magnitude of impact. Please note that bioturbation has no impact on sediment redistribution in
700 regions with low sink connectivity and topographic ruggedness. The relationship between the values of
701 environmental parameters and the impact of bioturbation is not linear: Bioturbation can have the same
702 impact on sediment redistribution at high or low values of an environmental parameter, but a contrasting
703 impact at middle values of this parameter (as in this case for elevation, slope or surface roughness).

5.Discussion

5.1 The inclusion of bioturbation increases model performance

707 Overall, our DMMF model including bioturbation performed much better than the model without
708 bioturbation. The DMMF model without bioturbation performed worse (RMSE of 1.18 kg ha^{-1} year^{-1} and
709 R^2 of 0.17) than the model with bioturbation (RMSE was 0.63 kg ha^{-1} year^{-1} and R^2 was 0.71).
710 We hence argue that the higher accuracy of our model can be explained with the inclusion of
711 bioturbation. This is confirmed by the fact that our model run without bioturbation performed similarly to

previously run models without bioturbation: In earlier studies, the accuracy of the MMF model reached an RMSE in between 4.9 and 8.2 kg ha^{-1} year^{-1}, with an estimated R^2 of in between 0.21 and 0.57 (Jong et al., 1999; Vigiak et al., 2005; López-Vicente et al., 2008; Vieira et al., 2014; Choi et al., 2017). However, we acknowledge that previous studies were all conducted in more temperate climate zones. To be able to compare our results with previous studies, we calculated the model performance considering solely the Mediterranean and humid climate zone, which are more similar in climate to the more temperate locations of previous studies. The performance of the model was still high ($R^2 = 0.72$, RMSE = 0.45 kg ha^{-1} year^{-1}), confirming the conclusion that bioturbation increased model performance. We compared the modelled impact of bioturbation on sediment redistribution with the impact of bioturbation estimated in previous studies. In the humid zone, our model predicted an erosion up to 3.5 kg m^{-2} year^{-1}. This estimation is in line with erosion rates established by in-situ measurements in other studies conducted in a more humid climate zone (between 1.5 kg m^{-2} year^{-1} and 3.7 kg m^{-2} year^{-1}) (Black and Montgomery, 1991; Yoo and Mudd, 2008; Yoo et al., 2005; Rutin, 1996). This also confirms the reliability of our approach. Previous authors estimated the impacts using rainfall simulators, erosion pins or splash boards. The measurements were conducted for a time period between 3 months and 3 years and the sites were revisited for each estimation. We do not compare our results with studies which previously applied models to estimate impacts of bioturbation, as, to our knowledge, none of the previous studies integrated vertebrate burrow structures into a soil erosion model and ran the model on a daily basis.

5.2 The relevance of bioturbation for sediment redistribution depends on the environmental context

On the hillslope catchment scale (1 ha), our study finds that bioturbation increases erosion in semi-arid and Mediterranean zone, accumulation in the arid zone and has no impact within the humid zone (Figure 6b). In contrast, bioturbation increases both, erosion, and accumulation, on the plot scale (1 m^2) (Figure 6a). On this scale, in the arid and semi-arid zone, sediment erosion and accumulation were predicted to be about equal (erosion and accumulation both up to 0.1 kg m^{-2} year^{-1} in the arid zone, and erosion and accumulation both up to 0.2 kg m^{-2} year^{-1} in the semi-arid zone (see Figure 6a)). Bioturbation marginally increased erosion and decreased accumulation in the semi-arid zone but reduced by twofold accumulation in the arid zone. In contrast, in the Mediterranean and humid zone, erosion was predicted to be almost double when compared to accumulation (predicted erosion up to 2.5 kg m^{-2} year$^{-1,}$, and accumulation up to 1.4 kg m^{-2} year^{-1}). Inclusion of bioturbation increased erosion up to 3 kg m^{-2} year$^{-1,}$ and accumulation up to 1.6 kg m^{-2} year^{-1} in the Mediterranean zone, while it had no significant effect in the humid zone. We argue that sediment redistribution due to bioturbation is heavily influenced by meso-topographic structures which determine the flow path of surface runoff and influence the infiltration processes. Due to this, the erosion and accumulation on the plots scale is heavier impacted by bioturbation with increasing surface runoff.

Our study found an increase of erosion in the semi-arid and Mediterranean climate zone to be between 6.5 % and 15.6 % due to bioturbation. Previous studies found that already a small increase of erosion has significant impacts on the whole hillslope catchment. A 10% increase in erosion rates over a 10-

year period can lead to significant changes in the landscape, including e.g. a 20-30% reduction in soil thickness and an increase in sediment transport in nearby rivers (Kuhn 2016).

According to our analysis, bioturbation increases erosion or accumulation of sediment mostly based on an interplay between topographic structures elevation, slope and TRI (Figure 10). Over all research sites, this study found that bioturbation leads to an increase in surface erosion in areas where erosional processes dominate (upper, and/or steeper slopes), and tends to increase sediment accumulation in areas where sediment is naturally deposited, e.g. lower slopes or shallow depressions (Figure 10). This finding is based on the fact that erosion in general is positively affected by slope, and negatively by surface roughness and vegetation (Rodríguez-Caballero et al., 2012; Wang et al., 2013; Kirols et al., 2015). Additionally, the redistribution of sediment is largely affected by topographic meso-/macroforms, such as rills or cliffs. These can be quantified by topographic ruggedness index (TRI) which describes the amount of elevation drop between adjusting cells of DEM (Wilson et al., 2007). At high values of this index, we would therefore expect high erosion rate, due to concentrated runoff within the connected rills or undisturbed flow of runoff from the cliffs downslope.

Our data show that one burrow provides up to 0.43 m^3 of additional loose sediment at the surface (Table 2), while the surface roughness increases up to 200 % (Grigusova et al., 2022). When including burrows into the model, at the slope values from 0 to 5 degrees, the presence of burrows had no impact on sediment redistribution. From 5 degrees onwards it increased sediment erosion proportionally to the slope of the hillside (an increased erosion from 0.4 g ha^{-1} year^{-1} in the semi-arid zone until up to 150 kg ha^{-1} year^{-1} in the Mediterranean zone, Fig. A3 – A6). Similarly, at locations with elevation drops ranging from 0 m until 0.2 m (lower TRI values), the presence of burrows had no impact. However, at locations with elevation drops of 0.2 until 0.5 m (higher TRI values), bioturbation increases sediment erosion by 1.5 kg ha^{-1} year^{-1} (Fig. A3 – A8). Lastly, bioturbation proportionally increased accumulation when the surface roughness values were above 0.5 (an increased accumulation from 0.2 g ha^{-1} year^{-1} in semi-arid zone until 5000 kg ha^{-1} year^{-1} in the Mediterranean zone, Fig. A3 – A6).

We conclude that in locations with slope values over 5 degrees, or at locations with sudden drops in elevation (high TRI), and connected rills, more sediment is eroding than accumulating. Here, additional surface sediments generated by bioturbators provides more source material for erosion and thus bioturbation increases sediment erosion at these locations (Figure 10 and 11). In contrast, at locations with a slope below 5 degrees, where processes are dominantly controlled by surface roughness, sediment accumulation caused by bioturbation increases proportionally when the surface roughness has a value above 0.5. This is likely because burrows through their above-ground structures heavily increase surface roughness (Grigusova et al., 2022), and hence the presence of bioturbating animals leads to an increase in sediment accumulation.

Additionally, we hypothesize that it is not only the additional availability of sediment on the surface and the topography of the vicinity which controls the contribution of bioturbation to sediment surface flux, but also the spatial distribution of animal burrows. We interpret that in locations with high burrow aggregation, surface flow might be redirected and centralized around the aggregates and thus increase sediment erosion in the areas adjacent burrow aggregates (Figure 11). This mechanism could explain why bioturbation promotes sediment erosion especially in the Mediterranean zone where burrows are

792 more aggregated. The relative role of burrow aggregation should be studied in detail and included in
793 future studies.
794
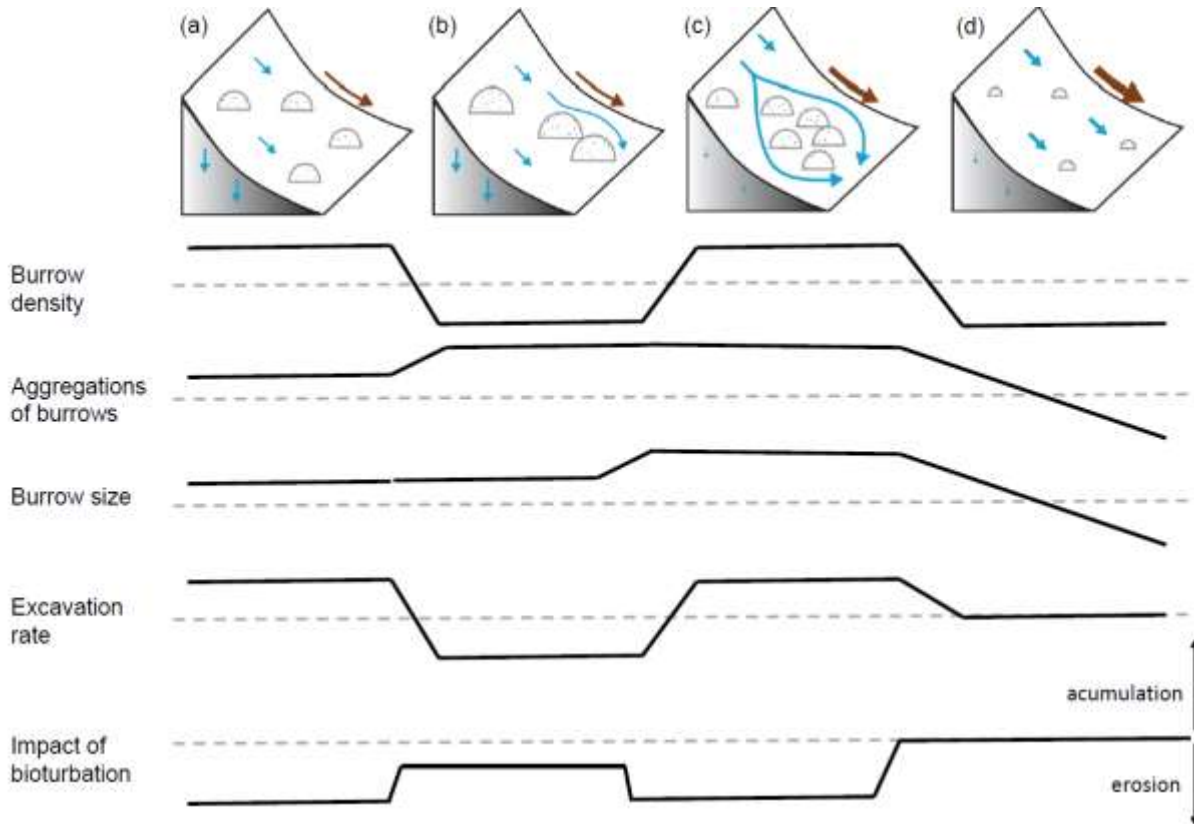
795
796 **Figure 11.** Context dependency of sediment redistribution. (a) Pan de Azúcar, (b) Santa Gracia, (c) La
797 Campana, and (d) Nahuelbuta. Brown arrows indicate the direction and magnitude of overall sediment
798 redistribution within each climate zone. Blue arrows indicate the direction of flow (runoff vs. infiltration).
799 Half-moons indicate the distribution and size of the burrows.
800
801

802 **6. Conclusion**
803 Our study found that the inclusion of vertebrate bioturbators' burrows into a soil erosion model
804 significantly increases its reliability. Vertebrate bioturbators increase sediment accumulation in the arid
805 climate zone, sediment erosion in the semi-arid and Mediterranean zone and have no impact on
806 sediment redistribution in the humid. Our study furthermore shows that the impact of bioturbation heavily
807 depends on the adjacent environmental parameters. The burrows increase sediment erosion at high
808 and low values of elevation, at high values of slope, sink connectivity and topography ruggedness, and
809 at low values of vegetation cover. The burrows increase accumulation at high values of surface
810 roughness and soil wetness. This means that overall, on geological time scales, as burrowing animals
811 increase both, erosion in steeper zones, and accumulation in areas with gentler slopes and higher
812 roughness, hillslope relief should become faster equalised and overall, more flat. This tendency is most
813 pronounced in the Mediterranean zone with high burrow density and excavation rates, as well as
814 comparably high precipitation rates.

815
816 **Funding:** This study was funded by the German Research Foundation, DFG [grant numbers
817 BE1780/52-1, LA3521/1-1, FA 925/12-1, BR 1293-18-1], and is part of the DFG Priority Programme
818 SPP 1803: EarthShape: Earth Surface Shaping by Biota, sub-project "Effects of bioturbation on rates
819 of vertical and horizontal sediment and nutrient fluxes".
820 **Institutional Review Board Statement:** Not applicable.
821 **Informed Consent Statement:** Not applicable.
822 **Acknowledgments:** We thank CONAF for the kind support provided during our field campaign.
823 **Competing interests:** There is no conflict of interest.
824 **Author contribution:** PG set up the model, analysed the data and wrote the manuscript draft; PG and
825 AL performed the measurements AL, JB, NF, RB, DK, PP, LP, CdR reviewed and edited the manuscript.
826 **Code/Data availability:** The estimated soil properties (DOI: 10.5678/wsrb-9f70), modelled sediment
827 redistribution (DOI: 10.5678/32wa-d179) and model code (https://gitlab.uni-marburg.de/fb19/ag-
828 bendix/model-sediment-redistribution-caused-by-bioturbating-animals) was published via LCRS data
829 services.
830 **Special Issue statement:** I would like to stress that the submission should be part of the Copernicus
831 special Issue (Earth surface shaping by biota (ESurf/BG/ESD/ESSD/SOIL inter-journal SI) initiated by
832 the EarthShape consortium.
833

834

835 burrows. The dashed line indicates the median value of each parameter for the first four parameters.
836

837 **Supplementary material**

838 **Table A1:** R^2 and RMSE of random forest models trained for the prediction of soil properties needed for
839 model parametrization. RMSE is root mean square error.

Variable	R^2	RMSE
Soil water content	0.80	0.05
Bulk density	0.60	0.22
Porosity	0.63	0.09
Silt	0.64	0.04
Middle silt	0.64	0.04
Sand	0.68	0.09
Middle sand	0.64	0.05
Organic components	0.77	0.05
Organic carbon	0.70	0.03

840

841 **Table A2.** Model sensitivity analysis. For the analysis, the minimum, maximum and mean value of each
842 parameter was calculated. The model was run for a hillslope catchment of 1km^2 with homogenous mean
843 parameters. Then, the minimum and maximum values of each parameter were tested. Each parameter
844 was stepwise changed to its minimum or maximum value while the remaining parameters stayed
845 homogenous. The significance of the parameter was estimated by a t-test conducted between the

 erosion estimated by the model with homogenous mean parameters and the erosion estimated by the

847 model with varying minimum and maximum parameter values. Only significant parameters are shown.

Parameter	mean value	min value	max value	mean erosion [kg m⁻¹]	Min erosion [kg m⁻¹]	Max erosion [kg m⁻¹]	Erosion [kg m⁻¹]
Precipitation [mm rainfall event⁻¹]	19.9	0.2	65.6	0.07	0	4.1	
clay content [%]	10.61	3.87	34.64	0.07	0.07	0.07	
silt content [%]	38.49	13.32	59.59	0.07	0.04	0.11	
sand content [%]	47.04	24.13	79.17	0.07	0.07	0.07	
water content [%]	3.87	2.38	12.68	0.07	0.09	0.06	
roughness [-]	0.97	0	236.8	0.07	0.34	0.01	
vegetation [%]	79.54	50.38	92.48	0.07	0.01	0.004	
Slope of DEM [°]	18.2	0	89.78	0.07	0	inf.	

848

849

850 **Table A3.** Summary of GAM models. We analyzed the impact of parameters within a 1-meter and 10-
851 meter distance from burrows. The Stars indicate p-values of the selected parameters. p*** < 0.001, p**
852 < 0.01, p* < 0.05, p. < 0.1. One GAM model was run per parameter. Only results for models with an
853 explained variance above 5 % are shown.

Parameters	Within 1 meter from burrows				Within 10 meters from burrows			
	PdA	SG	LC	NA	PdA	SG	LC	NA
Explained Variance	3.8 %	37 %	46 %	42 %	2.0 %	13 %	52 %	73 %
Burrow density	.				.			
Elevation			***	***	*		*	***
Slope		***					*	**
Aspect	.	**		*	*			.
Roughness		***					**	*

TPI							
TRI	**		**				
Plan curvature	.						.
Profile curv.	**	.					
NDVI		**			**		.
Sinks		*	***	*		*	
Wetness			**				
Flow direction							
Flow path							
Catchment	*			*			
Catchment slope	***		.				

854

855 **Table A4.** Review of studies which integrated any kind of bioturbation into models. Previous models
856 integrated either benthic, invertebrate or single species of vertebrate bioturbators. Models applied
857 either described the vertical soil mixing or long-term landscape evolution models. None of the previous
858 studies included vertebrate burrows of bioturbators into an erosion model which would be capable to
859 capture the daily redistribution processes.

References	Bioturbators	Integrated processes	Targeted process	Model
Francois et al. 1997, Francois et al. 2002, Kadko and Heath 1984, Croix et al. 2002 and several others	Various benthic bioturbators	Equations describing soil mixing within a floodplain	Vertical soil mixing within a floodplain	Mathematical equations
Orvain et al. 2006, Román – Sánchez et al. 2019, Orvain 2005, Orvain 2003, Sanford 2008 and several others	Various invertebrates	Equations describing vertical soil mixing	Influence of vertical soil mixing on lateral redistribution	Mathematical equations
Gabet 2000	Pocket gophers	Equation describing diffusion caused by gopher bioturbation	Relief changes over 40 000 years, lateral redistribution	Landscape evolution
Gabet et al. 2014	Pocket gophers	Equations describing sediment accumulation caused by gophers	Relocation of sediment to create Mima mounds	Landscape evolution
Temme and Vanwalleghem 2016	Not specified invertebrates	Bioturbation causes soil mixing between model layers. Mixing	Soil and landscape evolution	Landscape evolution

Vanwalleghem et al. 2013		is proportional to depth in the profile, soil thickness, and soil carbon content, and layer distance		Landscape evolution
Yoo and Mudd 2008		Bioturbation is considered as the cause of colluvial transport. Colluvial fluxes are calculated as a function of soil thickness and slope gradient on sloping grounds		Landscape evolution
Pelletier et al. 2013		Vertical soil mixing. Rate increases linearly with aboveground biomass.	creep including abiotic and bioturbation-driven transport	Landscape evolution
Van der Meij et al.2020		Vertical soil mixing. Rate depends on vegetation type.	Soil and landscape evolution	Landscape evolution
Our model	Vertebrates	The model includes burrow structure, adjusted soil properties and adjusted vegetation cover. Burrow distribution determined by machine learning.	Daily lateral sediment redistribution	Daily erosion model

860

861

862
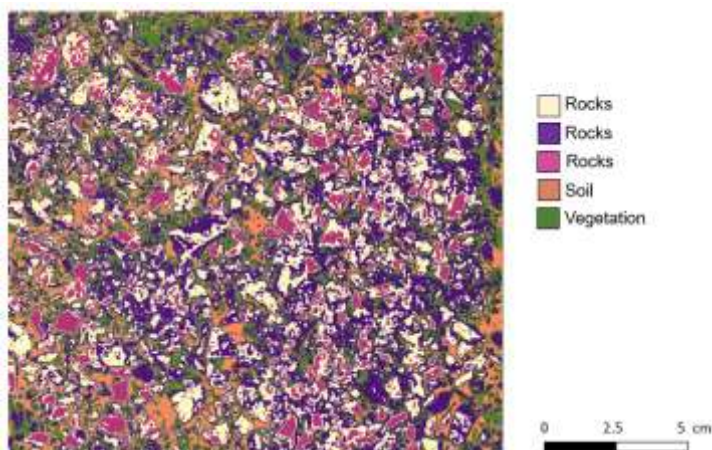
Figure A1. Example of the unsupervised k-means classification of the surface photo from La Campana. Original photo was taken by Paulina Grigusova. The collection of in-situ data is explained in section 3.1., the estimation of soil properties in section 3.2. The image was classified into 5 classes using unsupervised k-means classification; the land cover was then assigned manually. In some cases, like

867 in this case for rocks, multiple k-means classes stand for the same land cover. These were then unified

868 to the class "rocks".

869

870

871
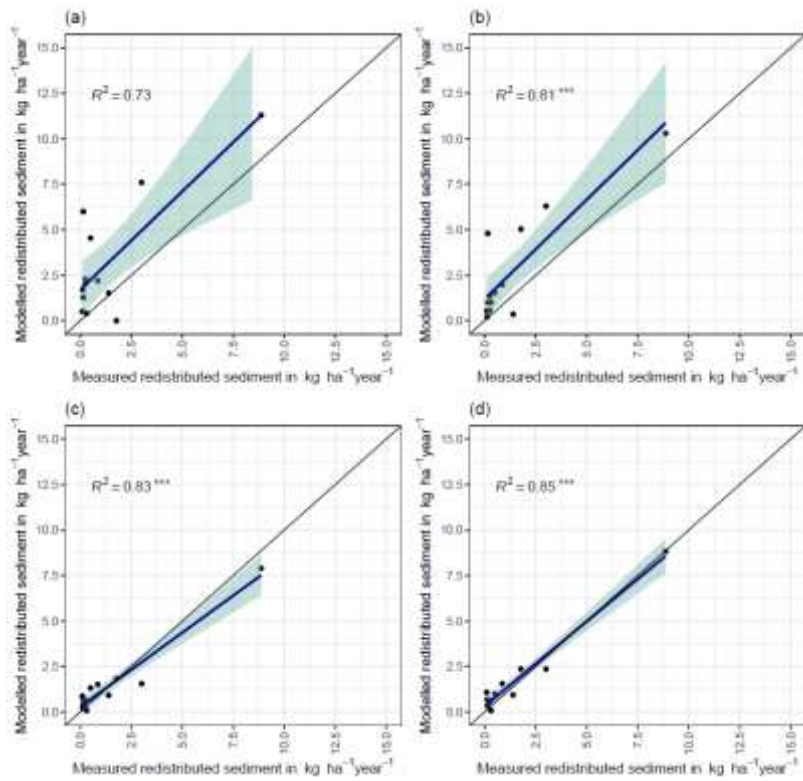
Figure A2. Measured and modelled redistributed sediment for different scenarios. (a) Model without

bioturbation. (b) Model with entrances. (c) Model with mounds. (d) model with burrows.

874

875

876

877

878

879
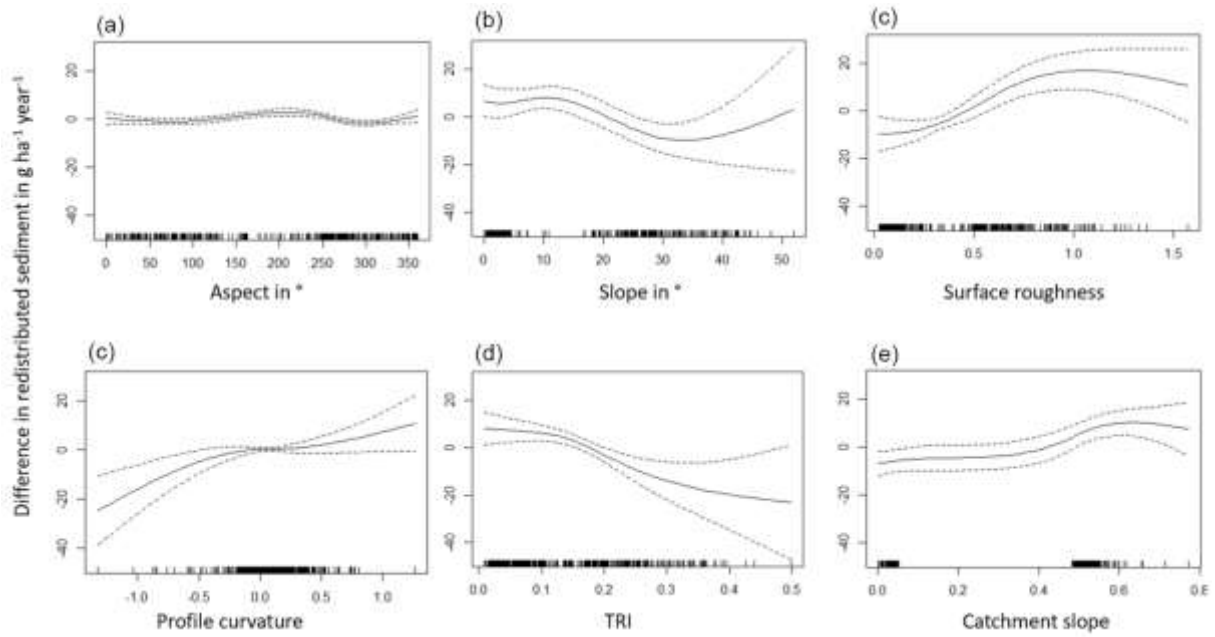
880 **Figure A3.** Environmental parameters influencing impact of bioturbation on sediment redistribution in
881 Santa Gracia within 1-meter distance from burrows. Positive values indicate bioturbation enhances
882 sediment accumulation at the respective parameter values, negative values indicate bioturbation
883 enhances sediment erosion at the respective parameter values.

884

885
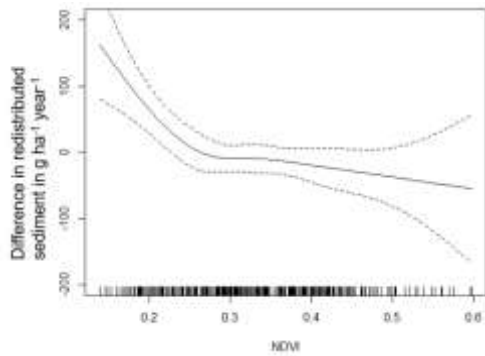
886 **Figure A4.** Environmental parameters influencing impact of bioturbation on sediment redistribution in
887 Santa Gracia within 10-meter distance from burrows. Positive values indicate bioturbation enhances
888 sediment accumulation at the respective parameter values, negative values indicate bioturbation
889 enhances sediment erosion at the respective parameter values.

890
891
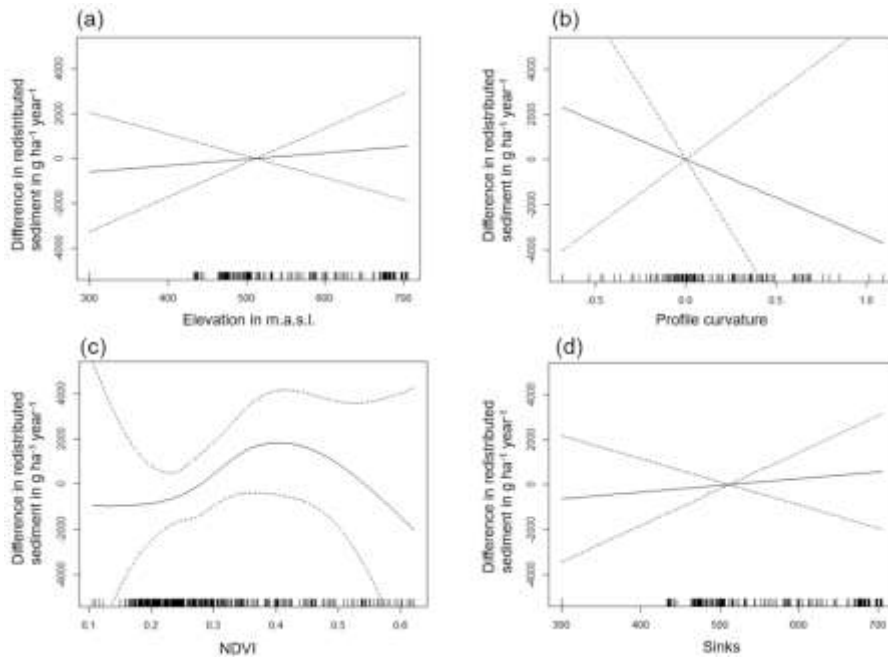
892
893 **Figure A5.** Environmental parameters influencing impact of bioturbation on sediment redistribution in
894 La Campana within 1-meter distance from burrows. Positive values indicate bioturbation enhances
895 sediment accumulation at the respective parameter values, negative values indicate bioturbation
896 enhances sediment erosion at the respective parameter values.

897
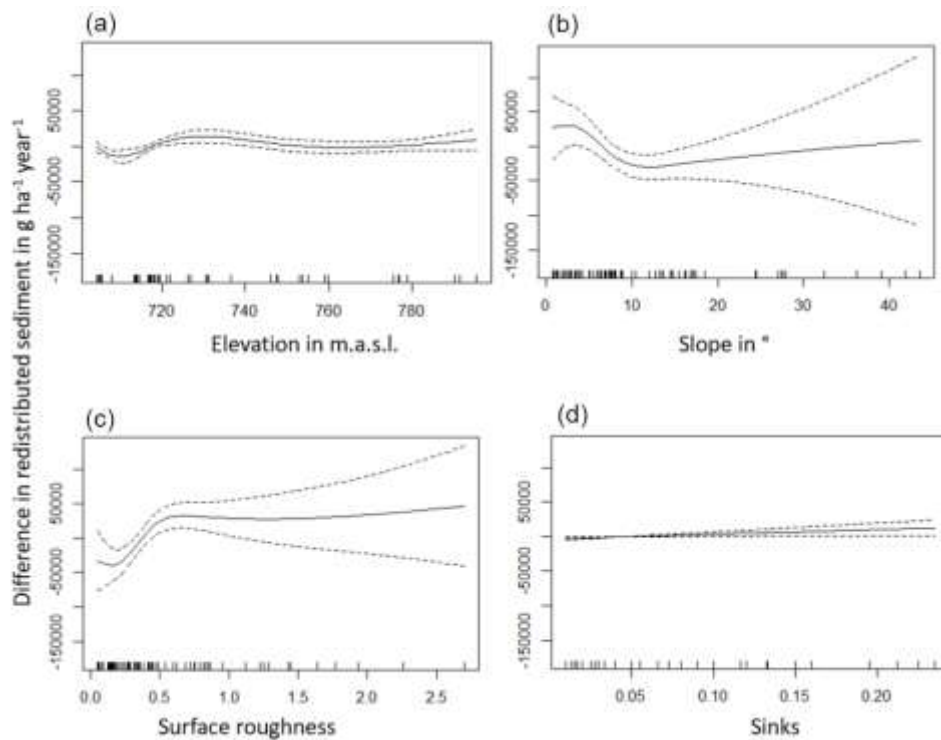
898
899 **Figure A6.** Environmental parameters influencing impact of bioturbation on sediment redistribution in
900 La Campana within 10-meter distance from burrows. Positive values indicate bioturbation enhances
901 sediment accumulation at the respective parameter values, negative values indicate bioturbation
902 enhances sediment erosion at the respective parameter values.

903

904
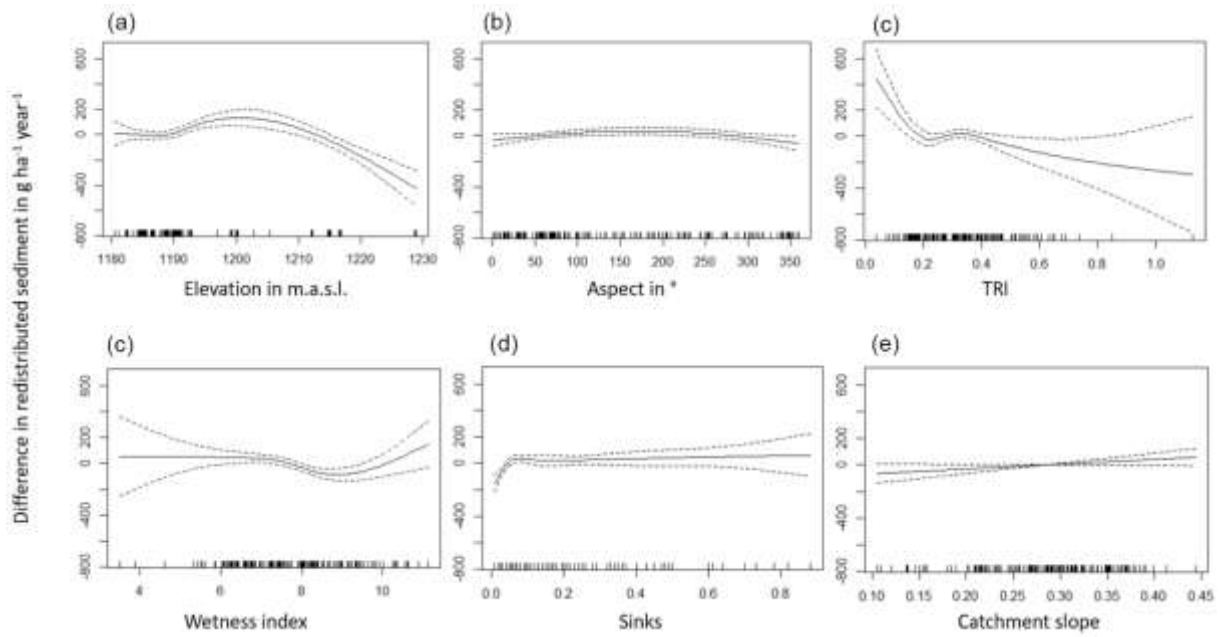
905

906 **Figure A7.** Environmental parameters influencing impact of bioturbation on sediment redistribution in
907 Nahuelbuta 1-meter distance from burrows. Positive values indicate bioturbation enhances sediment
908 accumulation at the respective parameter values, negative values indicate bioturbation enhances
909 sediment erosion at the respective parameter values.
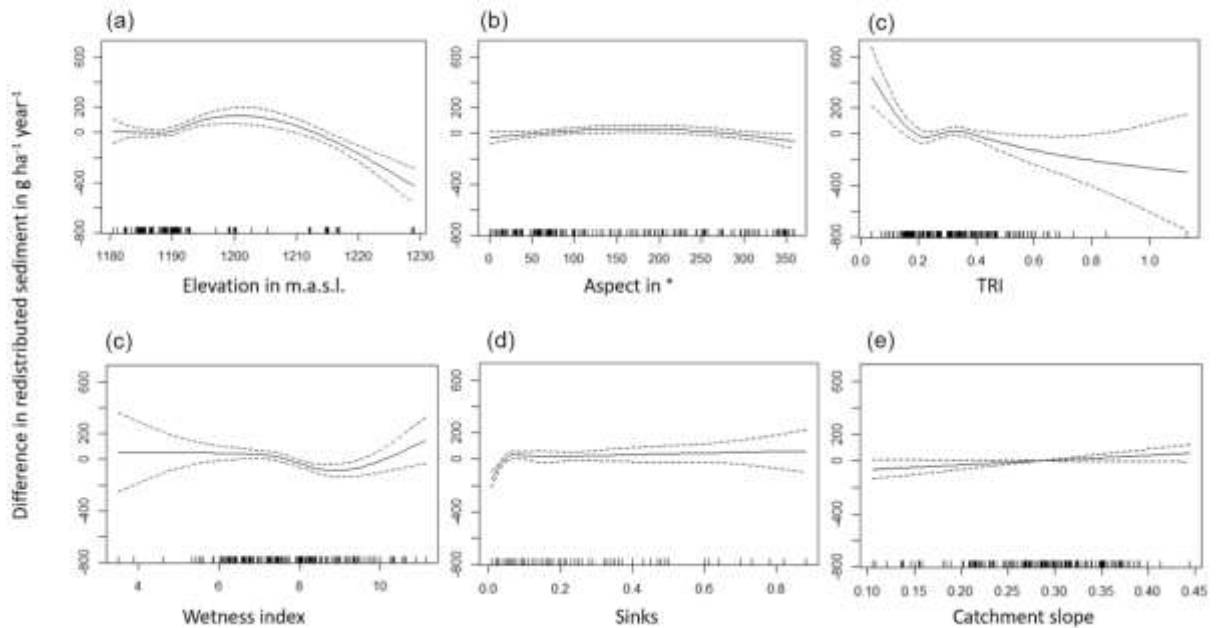
910

911 **Figure A8.** Environmental parameters influencing impact of bioturbation on sediment redistribution in
912 Nahuelbuta 10-meter distance from burrows. Positive values indicate bioturbation enhances sediment
913 accumulation at the respective parameter values, negative values indicate bioturbation enhances
914 sediment erosion at the respective parameter values.

915
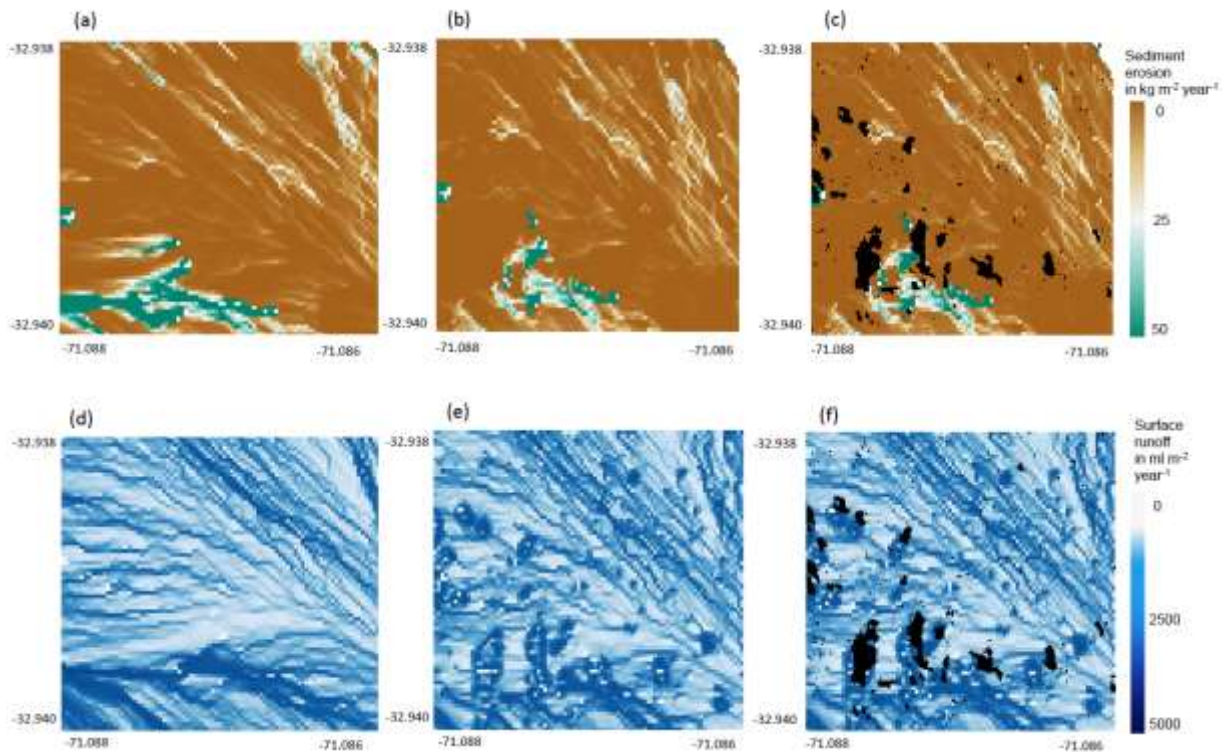
916

917 **Figure A9.** Burrow aggregation concentrates the runoff and increases erosion. Example for the north-

918 facing hillside in Mediterranean La Campana for the time period of one year. (a) Sediment erosion as

919 estimated by model without bioturbation. (b) Sediment erosion as estimated by model with bioturbation.

920 (c) Sediment erosion as estimated by model with bioturbation with predicted burrow locations. (d)

921 Surface runoff as estimated by model without bioturbation. (e) Surface runoff as estimated by model

922 with bioturbation. (f) Surface runoff as estimated by model including bioturbation and predicted burrow

923 locations. Black colour indicates, at least one burrow was located within this pixel. Four neighbouring

924 pixels which contain a burrow form a burrow aggregation.

925

926
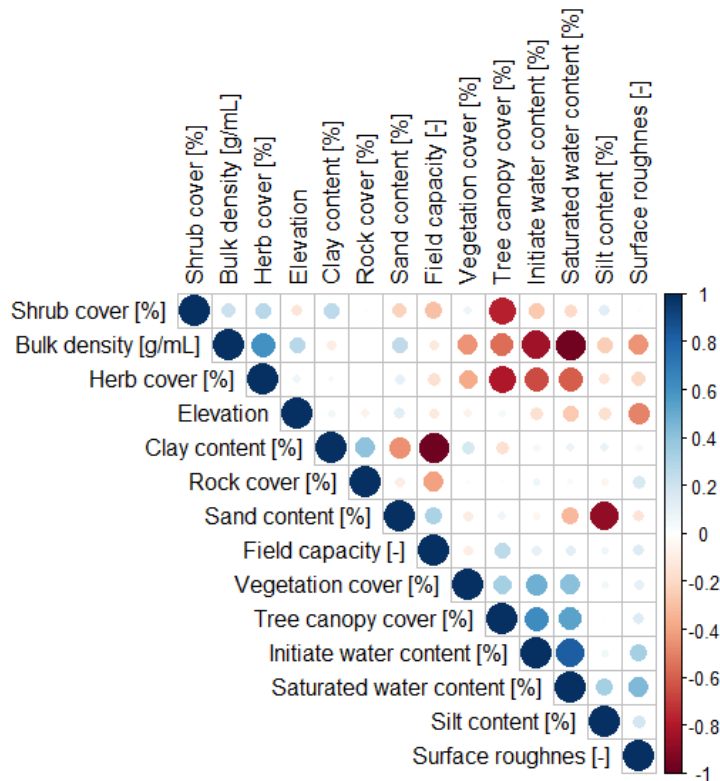
927 **Figure A10.** Correlation matrix between the model input parameters.

928

929

References

931 Anderson, R. S., Rajaram, H., and Anderson, S. P.: Climate driven coevolution of weathering profiles and
932   hillslope topography generates dramatic differences in critical zone architecture, Hydrol. Process., 33, 4–19,
933   https://doi.org/10.1002/hyp.13307, 2019.

934 Beasley, D. B., Huggins, L. F., and Monke, E. J.: ANSWERS: A Model for Watershed Planning, Transactions of the
935   ASAE, 23, 938–944, https://doi.org/10.13031/2013.34692, 1980.

936 Bernhard, N., Moskwa, L.-M., Schmidt, K., Oeser, R. A., Aburto, F., Bader, M. Y., Baumann, K., Blanckenburg, F.
937   von, Boy, J., van den Brink, L., Brucker, E., Büdel, B., Canessa, R., Dippold, M. A., Ehlers, T. A., Fuentes, J. P.,
938   Godoy, R., Jung, P., Karsten, U., Köster, M., Kuzyakov, Y., Leinweber, P., Neidhardt, H., Matus, F., Mueller,
939   C. W., Oelmann, Y., Oses, R., Osses, P., Paulino, L., Samolov, E., Schaller, M., Schmid, M., Spielvogel, S.,
940   Spohn, M., Stock, S., Stroncik, N., Tielbörger, K., Übernickel, K., Scholten, T., Seguel, O., Wagner, D., and
941   Kühn, P.: Pedogenic and microbial interrelations to regional climate and local topography: New insights from
942   a climate gradient (arid to humid) along the Coastal Cordillera of Chile, CATENA, 170, 335–355,
943   https://doi.org/10.1016/j.catena.2018.06.018, 2018.

944 Beven, K. J. and Kirkby, M. J.: A physically based, variable contributing area model of basin hydrology / Un
945   modèle à base physique de zone d'appel variable de l'hydrologie du bassin versant, Hydrological Sciences
946   Bulletin, 24, 43–69, https://doi.org/10.1080/02626667909491834, 1979.

947 Black, T. A. and Montgomery, D. R.: Sediment transport by burrowing mammals, Marin County, California, Earth
948   Surf. Process. Landforms, 16, 163–172, https://doi.org/10.1002/esp.3290160207, 1991.

949 Boudreau, B. P.: Mathematics of tracer mixing in sediments; I, Spatially-dependent, diffusive mixing, American
950   Journal of Science, 286, 161–198, https://doi.org/10.2475/ajs.286.3.161, 1986.

951 Boudreau, B. P.: The diffusion and telegraph equations in diagenetic modelling, Geochimica et Cosmochimica
952   Acta, 53, 1857–1866, https://doi.org/10.1016/0016-7037(89)90306-2, 1989.

953 Braun, J., Mercier, J., Guillocheau, F., and Robin, C.: A simple model for regolith formation by chemical
954   weathering, J. Geophys. Res. Earth Surf., 121, 2140–2171, https://doi.org/10.1002/2016JF003914, 2016.

955 Brosens, L., Campforts, B., Robinet, J., Vanacker, V., Opfergelt, S., Ameijeiras-Mariño, Y., Minella, J. P. G., and
956   Govers, G.: Slope Gradient Controls Soil Thickness and Chemical Weathering in Subtropical Brazil:
957   Understanding Rates and Timescales of Regional Soilscape Evolution Through a Combination of Field Data
958   and Modeling, J. Geophys. Res. Earth Surf., 125, 1, https://doi.org/10.1029/2019JF005321, 2020.

959 Carretier, S., Goddéris, Y., Delannoy, T., and Rouby, D.: Mean bedrock-to-saprolite conversion and erosion rates
960   during mountain growth and decline, Geomorphology, 209, 39–52,
961   https://doi.org/10.1016/j.geomorph.2013.11.025, 2014.

962 Cerqueira, R.: The Distribution of Didelphis in South America (Polyprotodontia, Didelphidae), Journal of
963   Biogeography, 12, 135, https://doi.org/10.2307/2844837, 1985.

964 Chen, M., Ma, L., Shao, M.'a., Wei, X., Jia, Y., Sun, S., Zhang, Q., Li, T., Yang, X., and Gan, M.: Chinese zokor
965   (Myospalax fontanierii) excavating activities lessen runoff but facilitate soil erosion – A simulation
966   experiment, CATENA, 202, 105248, https://doi.org/10.1016/j.catena.2021.105248, 2021.

967 Choi, K., Arnhold, S., Huwe, B., and Reineking, B.: Daily Based Morgan–Morgan–Finney (DMMF) Model: A
968   Spatially Distributed Conceptual Soil Erosion Model to Simulate Complex Soil Surface Configurations,
969   Water, 9, 278, https://doi.org/10.3390/w9040278, 2017.

970 Cohen, S., Willgoose, G., Svoray, T., Hancock, G., and Sela, S.: The effects of sediment transport, weathering, and
971   aeolian mechanisms on soil evolution, J. Geophys. Res. Earth Surf., 120, 260–274,
972   https://doi.org/10.1002/2014JF003186, 2015.

973 Cohen, S., Willgoose, G., and Hancock, G.: The mARM3D spatially distributed soil evolution model: Three-
974   dimensional model framework and analysis of hillslope and landform responses, J. Geophys. Res., 115, 191,
975   https://doi.org/10.1029/2009JF001536, 2010.

976 Coombes, M. A.: Biogeomorphology: diverse, integrative and useful, Earth Surf. Process. Landforms, 41, 2296–
977   2300, https://doi.org/10.1002/esp.4055, 2016.

978 Corenblit, D., Corbara, B., and Steiger, J.: Biogeomorphological eco-evolutionary feedback between life and
979   geomorphology: a theoretical framework using fossorial mammals, Die Naturwissenschaften, 108, 55,
980   https://doi.org/10.1007/s00114-021-01760-y, 2021.

981 Debruyn, L. A.L. and Conacher, A. J.: The bioturbation activity of ants in agricultural and naturally vegetated
982   habitats in semiarid environments, Soil Res., 32, 555, https://doi.org/10.1071/SR9940555, 1994.

983 Devia, G. K., Ganasri, B. P., and Dwarakish, G. S.: A Review on Hydrological Models, Aquatic Procedia, 4, 1001–
984   1007, https://doi.org/10.1016/j.aqpro.2015.02.126, 2015.

985 Durner, W., Iden, S. C., and Unold, G. von: The integral suspension pressure method (ISP) for precise particle-size
986   analysis by gravitational sedimentation, Water Resour. Res., 53, 33–48, https://doi.org/10.1002/2016WR019830,
987   2017.

988 Eccard, J. A. and Herde, A.: Seasonal variation in the behaviour of a short-lived rodent, BMC ecology, 13, 43,
989   https://doi.org/10.1186/1472-6785-13-43, 2013.

990 Ferro, L. I. and Barquez, R. M.: Species Richness of Nonvolant Small Mammals Along Elevational Gradients in
991   Northwestern Argentina, Biotropica, 41, 759–767, https://doi.org/10.1111/j.1744-7429.2009.00522.x, 2009.

992 Foster, D. W.: BIOTURB: A FORTRAN program to simulate the effects of bioturbation on the vertical distribution
993   of sediment, Computers & Geosciences, 11, 39–54, https://doi.org/10.1016/0098-3004(85)90037-8, 1985.

François, F., Poggiale, J.-C., Durbec, J.-P., and Stora, G.: A New Approach for the Modelling of Sediment Reworking Induced by a Macrobenthic Community, Acta Biotheoretica, 45, 295–319, https://doi.org/10.1023/A:1000636109604, 1997.

Gabet, E. J.: Gopher bioturbation: field evidence for non-linear hillslope diffusion, Earth Surf. Process. Landforms, 25, 1419–1428, https://doi.org/10.1002/1096-9837(200012)25:13<1419:AID-ESP148>3.0.CO;2-1, 2000.

Gabet, E. J., Perron, J. T., and Johnson, D. L.: Biotic origin for Mima mounds supported by numerical modeling, Geomorphology, 206, 58–66, https://doi.org/10.1016/j.geomorph.2013.09.018, 2014.

Gabet, E. J., Reichman, O. J., and Seabloom, E. W.: The Effects of Bioturbation on Soil Processes and Sediment Transport, Annu. Rev. Earth Planet. Sci., 31, 249–273, https://doi.org/10.1146/annurev.earth.31.100901.141314, 2003.

Gray, H. J., Keen-Zebert, A., Furbish, D. J., Tucker, G. E., and Mahan, S. A.: Depth-dependent soil mixing persists across climate zones, Proceedings of the National Academy of Sciences of the United States of America, 117, 8750–8756, https://doi.org/10.1073/pnas.1914140117., 2020.

Grigusova, P., Larsen, A., Achilles, S., Brandl, R., del Río, C., Farwig, N., Kraus, D., Paulino, L., Pliscoff, P., Übernickel, K., and Bendix, J.: Higher sediment redistribution rates related to burrowing animals than previously assumed as revealed by time-of-flight-based monitoring, Earth Surf. Dynam., 10, 1273–1301, https://doi.org/10.5194/esurf-10-1273-2022, 2022.

Grigusova, P., Larsen, A., Achilles, S., Klug, A., Fischer, R., Kraus, D., Übernickel, K., Paulino, L., Pliscoff, P., Brandl, R., Farwig, N., and Bendix, J.: Area-Wide Prediction of Vertebrate and Invertebrate Hole Density and Depth across a Climate Gradient in Chile Based on UAV and Machine Learning, Drones, 5, 86, https://doi.org/10.3390/drones5030086, 2021.

Hakonson, T. E.: The Effects of Pocket Gopher Burrowing on Water Balance and Erosion from Landfill Covers, J. environ. qual., 28, 659–665, https://doi.org/10.2134/jeq1999.00472425002800020033x, 1999.

Hall, K., Boelhouwers, J., and Driscoll, K.: Animals as Erosion Agents in the Alpine Zone: Some Data and Observations from Canada, Lesotho, and Tibet, Arctic, Antarctic, and Alpine Research, 31, 436–446, https://doi.org/10.1080/15230430.1999.12003328, 1999.

Hancock, G. and Lowry, J.: Quantifying the influence of rainfall, vegetation and animals on soil erosion and hillslope connectivity in the monsoonal tropics of northern Australia, Earth Surf. Process. Landforms, 46, 2110–2123, https://doi.org/10.1002/esp.5147, 2021.

Hazelhoff, L., van Hoof, P., Imeson, A. C., and Kwaad, F. J. P. M.: The exposure of forest soil to erosion by earthworms, Earth Surf. Process. Landforms, 6, 235–250, https://doi.org/10.1002/esp.3290060305, 1981.

Horn, B.K.P.: Hill shading and the reflectance map, Proc. IEEE, 69, 14–47, https://doi.org/10.1109/PROC.1981.11918, 1981.

Imeson, A. C. and Kwaad, F. J. P. M.: Some Effects of Burrowing Animals on Slope Processes in the Luxembourg Ardennes, Geografiska Annaler: Series A, Physical Geography, 58, 317–328, https://doi.org/10.1080/04353676.1976.11879941, 1976.

Istanbulluoglu, E.: Vegetation-modulated landscape evolution: Effects of vegetation on landscape processes, drainage density, and topography, J. Geophys. Res., 110, 11, https://doi.org/10.1029/2004JF000249, 2005.

Jimenez, J. E., Feinsinger, P., and Jaksi, F. M.: Spatiotemporal Patterns of an Irruption and Decline of Small Mammals in Northcentral Chile, Journal of Mammalogy, 73, 356–364, https://doi.org/10.2307/1382070, 1992.

Jong, S. M. de, Paracchini, M. L., Bertolo, F., Folving, S., Megier, J., and Roo, A.P.J. de: Regional assessment of soil erosion using the distributed model SEMMED and remotely sensed data, CATENA, 37, 291–308, https://doi.org/10.1016/S0341-8162(99)00038-7, 1999.

Jumars, P. A., Nowell, A. R.M., and Self, R. F.L.: A simple model of flow—Sediment—Organism interaction, Marine Geology, 42, 155–172, https://doi.org/10.1016/0025-3227(81)90162-6, 1981.

Kadko, D. and Heath, G. R.: Models of depth-dependent bioturbation at MANOP Site H in the eastern equatorial Pacific, J. Geophys. Res., 89, 6567, https://doi.org/10.1029/JC089iC04p06567, 1984.

Katzman, E. A., Zaytseva, E. A., Feoktistova, N. Y., Tovpinetz, N. N., Bogomolov, P. L., Potashnikova, E. V., and Surov, A. V.: Seasonal Changes in Burrowing of the Common Hamster (Cricetus cricetus L., 1758) (Rodentia: Cricetidae) in the City, PJE, 17, 251–258, https://doi.org/10.18500/1684-7318-2018-3-251-258, 2018.

Kinlaw, A. and Grasmueck, M.: Evidence for and geomorphologic consequences of a reptilian ecosystem engineer: The burrowing cascade initiated by the Gopher Tortoise, Geomorphology, 157-158, 108–121, https://doi.org/10.1016/j.geomorph.2011.06.030, 2012.

Kirols, H. S., Kevorkov, D., Uihlein, A., and Medraj, M.: The effect of initial surface roughness on water droplet erosion behaviour, Wear, 342-343, 198–209, https://doi.org/10.1016/j.wear.2015.08.019, 2015.

Kraus, D., Brandl, R., Achilles, S., Bendix, J., Grigusova, P., Larsen, A., Pliscoff, P., Übernickel, K., and Farwig, N.: Vegetation and vertebrate abundance as drivers of bioturbation patterns along a climate gradient, PloS one, 17, e0264408, https://doi.org/10.1371/journal.pone.0264408, 2022.

Kügler, M., Hoffmann, T. O., Beer, A. R., Übernickel, K., Ehlers, T. A., Scherler, D., and Eichel, J.: (LiDAR) 3D Point Clouds and Topographic Data from the Chilean Coastal Cordillera, 2022.

La Croix, A. D., Gingras, M. K., Dashtgard, S. E., and Pemberton, S. G.: Computer modeling bioturbation: The creation of porous and permeable fluid-flow pathways, Bulletin, 96, 545–556, https://doi.org/10.1306/07141111038, 2012.

Larsen, A., Nardin, W., Lageweg, W. I., and Bätz, N.: Biogeomorphology, quo vadis? On processes, time, and space in biogeomorphology, Earth Surf. Process. Landforms, 46, 12–23, https://doi.org/10.1002/esp.5016, 2021.

Le Hir, P., Monbet, Y., and Orvain, F.: Sediment erodability in sediment transport modelling: Can we account for biota effects?, Continental Shelf Research, 27, 1116–1142, https://doi.org/10.1016/j.csr.2005.11.016, 2007.

Lehnert, L. W., Thies, B., Trachte, K., Achilles, S., Osses, P., Baumann, K., Schmidt, J., Samolov, E., Jung, P., Leinweber, P., Karsten, U., Büdel, B., and Bendix, J.: A Case Study on Fog/Low Stratus Occurrence at Las Lomitas, Atacama Desert (Chile) as a Water Source for Biological Soil Crusts, Aerosol Air Qual. Res., 18, 254-26, https://doi.org/10.4209/aaqr.2017.01.0021, 2018.

Li, G., Li, X., Li, J., Chen, W., Zhu, H., Zhao, J., and Hu, X.: Influences of Plateau Zokor Burrowing on Soil Erosion and Nutrient Loss in Alpine Meadows in the Yellow River Source Zone of West China, Water, 11, 2258, https://doi.org/10.3390/w11112258, 2019a.

Li, T. C., Shao, M. A., Jia, Y. H., Jia, X. X., Huang, L. M., and Gan, M.: Small-scale observation on the effects of burrowing activities of ants on soil hydraulic processes, Eur J Soil Sci, 70, 236–244, https://doi.org/10.1111/ejss.12748, 2019b.

Li, T., Shao, M.'a., Jia, Y., Jia, X., and Huang, L.: Small-scale observation on the effects of the burrowing activities of mole crickets on soil erosion and hydrologic processes, Agriculture, Ecosystems & Environment, 261, 136–143, https://doi.org/10.1016/j.agee.2018.04.010, 2018.

Li, Z. and Zhang, J.: Calculation of Field Manning's Roughness Coefficient, Agricultural Water Management, 49, 153–161, https://doi.org/10.1016/S0378-3774(00)00139-6, 2001.

Lilhare, R., Garg, V., and Nikam, B. R.: Application of GIS-Coupled Modified MMF Model to Estimate Sediment Yield on a Watershed Scale, J. Hydrol. Eng., 20, 745, https://doi.org/10.1061/(ASCE)HE.1943-5584.0001063, 2015.

1079   López-Vicente, M., Navas, A., and Machín, J.: Modelling soil detachment rates in rainfed agrosystems in the
1080   south-central Pyrenees, Agricultural Water Management, 95, 1079–1089,
1081   https://doi.org/10.1016/j.agwat.2008.04.004, 2008.

1082   Malizia, A. I.: Population dynamics of the fossorial rodent Ctenomys talarum (Rodentia: Octodontidae), Journal
1083   of Zoology, 244, 545–551, https://doi.org/10.1111/j.1469-7998.1998.tb00059.x, 1998.

1084   Meserve, P. L.: Trophic Relationships among Small Mammals in a Chilean Semiarid Thorn Scrub Community,
1085   Journal of Mammalogy, 62, 304–314, https://doi.org/10.2307/1380707, 1981.

1086   Meyer, H., Reudenbach, C., Hengl, T., Katurji, M., and Nauss, T.: Improving performance of spatio-temporal
1087   machine learning models using forward feature selection and target-oriented validation, Environmental
1088   Modelling & Software, 101, 1–9, https://doi.org/10.1016/j.envsoft.2017.12.001, 2018.

1089   Meysman, F. J. R., Boudreau, B. P., and Middelburg, J. J.: Relations between local, nonlocal, discrete and
1090   continuous models of bioturbation, J Mar Res, 61, 391–410, https://doi.org/10.1357/002224003322201241, 2003.

1091   Milstead, W. B., Meserve, P. L., Campanella, A., Previtali, M. A., Kelt, D. A., and Gutiérrez, J. R.: Spatial Ecology
1092   of Small Mammals in North-central Chile: Role of Precipitation and Refuges, Journal of Mammalogy, 88,
1093   1532–1538, https://doi.org/10.1644/16-MAMM-A-407R.1, 2007.

1094   Monteverde, M. J. and Piudo, L.: Activity Patterns of the Culpeo Fox (Lycalopex Culpaeus Magellanica) in a
1095   Non-Hunting Area of Northwestern Patagonia, Argentina, Mammal Study, 36, 119–125,
1096   https://doi.org/10.3106/041.036.0301, 2011.

1097   Morgan, R. P. C. and Duzant, J. H.: Modified MMF (Morgan–Morgan–Finney) model for evaluating effects of
1098   crops and vegetation cover on soil erosion, Earth Surf. Process. Landforms, 33, 90–106,
1099   https://doi.org/10.1002/esp.1530, 2008.

1100   Morgan, R. P. C., Quinton, J. N., Smith, R. E., Govers, G., Poesen, J. W. A., Auerswald, K., Chisci, G., Torri, D., and
1101   Styczen, M. E.: The European Soil Erosion Model (EUROSEM): a dynamic approach for predicting sediment
1102   transport from fields and small catchments, Earth Surf. Process. Landforms, 23, 527–544,
1103   https://doi.org/10.1002/(SICI)1096-9837(199806)23:6<527:AID-ESP868>3.0.CO;2-5, 1998.

1104   Morgan, R.P.C.: A simple approach to soil loss prediction: a revised Morgan–Morgan–Finney model, CATENA,
1105   44, 305–322, https://doi.org/10.1016/S0341-8162(00)00171-5, 2001.

1106   Morgan, R.P.C., Morgan, D.D.V., and Finney, H. J.: A predictive model for the assessment of soil erosion risk,
1107   Journal of Agricultural Engineering Research, 30, 245–253, https://doi.org/10.1016/S0021-8634(84)80025-6,
1108   1984.

1109   Nearing, M. A., Foster, G. R., Lane, L. J., and Finkner, S. C.: A Process-Based Soil Erosion Model for USDA-Water
1110   Erosion Prediction Project Technology, Transactions of the ASAE, 32, 1587–1593,
1111   https://doi.org/10.13031/2013.31195, 1989.

1112   Nkem, J. N., Lobry de Bruyn, L. A., Grant, C. D., and Hulugalle, N. R.: The impact of ant bioturbation and
1113   foraging activities on adjacent soil properties, Pedobiologia, 44, 609–621, https://doi.org/10.1078/S0031-
1114   4056(04)70075-X, 2000.

1115   Oeser, R. A., Stroncik, N., Moskwa, L.-M., Bernhard, N., Schaller, M., Canessa, R., van den Brink, L., Köster, M.,
1116   Brucker, E., Stock, S., Fuentes, J. P., Godoy, R., Matus, F. J., Oses Pedraza, R., Osses McIntyre, P., Paulino, L.,
1117   Seguel, O., Bader, M. Y., Boy, J., Dippold, M. A., Ehlers, T. A., Kühn, P., Kuzyakov, Y., Leinweber, P.,
1118   Scholten, T., Spielvogel, S., Spohn, M., Übernickel, K., Tielbörger, K., Wagner, D., and Blanckenburg, F. von:
1119   Chemistry and microbiology of the Critical Zone along a steep climate and vegetation gradient in the Chilean
1120   Coastal Cordillera, CATENA, 170, 183–203, https://doi.org/10.1016/j.catena.2018.06.002, 2018.

1121   Orvain, F., Sauriau, P.-G., Bacher, C., and Prineau, M.: The influence of sediment cohesiveness on bioturbation
1122   effects due to Hydrobia ulvae on the initial erosion of intertidal sediments: A study combining flume and
1123   model approaches, Journal of Sea Research, 55, 54–73, https://doi.org/10.1016/j.seares.2005.10.002, 2006.

1124 Pelletier, J. D., Barron-Gafford, G. A., Breshears, D. D., Brooks, P. D., Chorover, J., Durcik, M., Harman, C. J.,
1125   Huxman, T. E., Lohse, K. A., Lybrand, R., Meixner, T., McIntosh, J. C., Papuga, S. A., Rasmussen, C., Schaap,
1126   M., Swetnam, T. L., and Troch, P. A.: Coevolution of nonlinear trends in vegetation, soils, and topography
1127   with elevation and slope aspect: A case study in the sky islands of southern Arizona, J. Geophys. Res. Earth
1128   Surf., 118, 741–758, https://doi.org/10.1002/jgrf.20046, 2013.

1129 Penman, H.: Natural evaporation from open water, hare soil and grass, Proceedings of the Royal Society of
1130   London. Series A, Mathematical and physical sciences, 193, 120–145, https://doi.org/10.1098/rspa.1948.0037,
1131   1948.

1132 Pollacco, J. A. P.: A generally applicable pedotransfer function that estimates field capacity and permanent
1133   wilting point from soil texture and bulk density, Can. J. Soil. Sci., 88, 761–774,
1134   https://doi.org/10.4141/CJSS07120, 2008.

1135 Qin, Y., Yi, S., Ding, Y., Qin, Y., Zhang, W., Sun, Y., Hou, X., Yu, H., Meng, B., Zhang, H., Chen, J., and Wang, Z.:
1136   Effects of plateau pikas' foraging and burrowing activities on vegetation biomass and soil organic carbon of
1137   alpine grasslands, Plant Soil, 458, 201–216, https://doi.org/10.1007/s11104-020-04489-1, 2021.

1138 Reichman, O. J. and Seabloom, E. W.: The role of pocket gophers as subterranean ecosystem engineers, Trends in
1139   Ecology & Evolution, 17, 44–49, https://doi.org/10.1016/S0169-5347(01)02329-1, 2002.

1140 Renard, K., Foster, G., Weesies, G., and Porter, J.: RUSLE: The Revised Universal Soil Loss Equation, Journal of
1141   Soil Water Conservation, 30–33, 1991.

1142 Ridd, P. V.: Flow Through Animal Burrows in Mangrove Creeks, Estuarine, Coastal and Shelf Science, 43, 617–
1143   625, https://doi.org/10.1006/ecss.1996.0091, 1996.

1144 Rodríguez-Caballero, E., Cantón, Y., Chamizo, S., Afana, A., and Solé-Benet, A.: Effects of biological soil crusts on
1145   surface roughness and implications for runoff and erosion, Geomorphology, 145-146, 81–89,
1146   https://doi.org/10.1016/j.geomorph.2011.12.042, 2012.

1147 Román-Sánchez, A., Reimann, T., Wallinga, J., and Vanwalleghem, T.: Bioturbation and erosion rates along the
1148   soil-hillslope conveyor belt, part 1: Insights from single-grain feldspar luminescence, Earth Surf. Process.
1149   Landforms, 44, 2051–2065, https://doi.org/10.1002/esp.4628, 2019.

1150 ROO, A. P. J. de, WESSELING, C. G., and RITSEMA, C. J.: LISEM: A SINGLE-EVENT PHYSICALLY BASED
1151   HYDROLOGICAL AND SOIL EROSION MODEL FOR DRAINAGE BASINS. I: THEORY, INPUT AND
1152   OUTPUT, Hydrol. Process., 10, 1107–1117, https://doi.org/10.1002/(SICI)1099-1085(199608)10:8<1107:AID-
1153   HYP415>3.0.CO;2-4, 1996.

1154 Rutin, J.: The burrowing activity of scorpions (Scorpio maurus palmatus) and their potential contribution to the
1155   erosion of Hamra soils in Karkur, central Israel, Geomorphology, 15, 159–168, https://doi.org/10.1016/0169-
1156   555X(95)00120-T, 1996.

1157 Sanford, L. P.: Modeling a dynamically varying mixed sediment bed with erosion, deposition, bioturbation,
1158   consolidation, and armoring, Computers & Geosciences, 34, 1263–1283,
1159   https://doi.org/10.1016/j.cageo.2008.02.011, 2008.

1160 Schiffers, K., Teal, L. R., Travis, J. M. J., and Solan, M.: An open source simulation model for soil and sediment
1161   bioturbation, PloS one, 6, e28028, https://doi.org/10.1371/journal.pone.0028028, 2011.

1162 Shannon, C. E.: A Mathematical Theory of Communication, Bell System Technical Journal, 27, 379–423,
1163   https://doi.org/10.1002/j.1538-7305.1948.tb01338.x, 1948.

1164 Shull, D. H.: Transition-matrix model of bioturbation and radionuclide diagenesis, Limnol. Oceanogr., 46, 905–
1165   916, https://doi.org/10.4319/lo.2001.46.4.0905, 2001.

1166 Simonetti, J. A.: Microhabitat Use by Small Mammals in Central Chile, Oikos, 56, 309,
1167   https://doi.org/10.2307/3565615, 1989.

Soetaert, K., Herman, P. M. J., Middelburg, J. J., Heip, C., deStigter, H. S., van Weering, T. C. E., Epping, E., and Helder, W.: Modeling ^{210}Pb-derived mixing activity in ocean margin sediments: Diffusive versus nonlocal mixing, J Mar Res, 54, 1207–1227, https://doi.org/10.1357/0022240963213808, 1996.

Taylor, A. R., Lenoir, L., Vegerfors, B., and Persson, T.: Ant and Earthworm Bioturbation in Cold-Temperate Ecosystems, Ecosystems, 22, 981–994, https://doi.org/10.1007/s10021-018-0317-2, 2019.

Temme, A. J.A.M. and Vanwalleghem, T.: LORICA – A new model for linking landscape and soil profile evolution: Development and sensitivity analysis, Computers & Geosciences, 90, 131–143, https://doi.org/10.1016/j.cageo.2015.08.004, 2016.

Tews, J., Brose, U., Grimm, V., Tielbörger, K., Wichmann, M. C., Schwager, M., and Jeltsch, F.: Animal species diversity driven by habitat heterogeneity/diversity: the importance of keystone structures, Journal of Biogeography, 31, 79–92, https://doi.org/10.1046/j.0305-0270.2003.00994.x, 2004.

Tomasella, J., Hodnett, M. G., and Rossato, L.: Pedotransfer Functions for the Estimation of Soil Water Retention in Brazilian Soils, Soil Sci. Soc. Am. J., 64, 327–338, https://doi.org/10.2136/sssaj2000.641327x, 2000.

Trauth, M. H.: TURBO: a dynamic-probabilistic simulation to study the effects of bioturbation on paleoceanographic time series, Computers & Geosciences, 24, 433–441, https://doi.org/10.1016/S0098-3004(98)00019-3, 1998.

Tucker, G. E. and Hancock, G. R.: Modelling landscape evolution, Earth Surf. Process. Landforms, 35, 28–50, https://doi.org/10.1002/esp.1952, 2010.

Übernickel, K., Pizarro-Araya, J., Bhagavathula, S., Paulino, L., and Ehlers, T. A.: Reviews and syntheses: Composition and characteristics of burrowing animals along a climate and ecological gradient, Chile, Biogeosciences, 18, 5573–5594, https://doi.org/10.5194/bg-18-5573-2021, 2021a.

Übernickel, K., Ehlers, T. A., Paulino, L., and Fuentes Espoz, J.-P.: Time series of meteorological stations on an elevational gradient in National Park La Campana, Chile, 2021b.

Vanwalleghem, T., Stockmann, U., Minasny, B., and McBratney, A. B.: A quantitative model for integrating landscape evolution and soil formation, J. Geophys. Res. Earth Surf., 118, 331–347, https://doi.org/10.1029/2011JF002296, 2013.

Vieira, D.C.S., Prats, S. A., Nunes, J. P., Shakesby, R. A., Coelho, C.O.A., and Keizer, J. J.: Modelling runoff and erosion, and their mitigation, in burned Portuguese forest using the revised Morgan–Morgan–Finney model, Forest Ecology and Management, 314, 150–165, https://doi.org/10.1016/j.foreco.2013.12.006, 2014.

Vigiak, O., Okoba, B. O., Sterk, G., and Groenenberg, S.: Modelling catchment-scale erosion patterns in the East African Highlands, Earth Surf. Process. Landforms, 30, 183–196, https://doi.org/10.1002/esp.1174, 2005.

Voiculescu, M., Ianăş, A.-N., and Germain, D.: Exploring the impact of snow vole (Chionomys nivalis) burrowing activity in the Făgăraş Mountains, Southern Carpathians (Romania): Geomorphic characteristics and sediment budget, CATENA, 181, 104070, https://doi.org/10.1016/j.catena.2019.05.016, 2019.

Wang, B., Zheng, F., Römkens, M. J.M., and Darboux, F.: Soil erodibility for water erosion: A perspective and Chinese experiences, Geomorphology, 187, 1–10, https://doi.org/10.1016/j.geomorph.2013.01.018, 2013.

Wei, X., Li, S., Yang, P., and Cheng, H.: Soil erosion and vegetation succession in alpine Kobresia steppe meadow caused by plateau pika—A case study of Nagqu County, Tibet, Chin. Geograph.Sc., 17, 75–81, https://doi.org/10.1007/s11769-007-0075-0, 2007.

Welivitiya, W. D. D. P., Willgoose, G. R., and Hancock, G. R.: A coupled soilscape–landform evolution model: model formulation and initial results, Earth Surf. Dynam., 7, 591–607, https://doi.org/10.5194/esurf-7-591-2019, 2019.

1210 Wheatcroft, R. A., Jumars, P. A., Smith, C. R., and Nowell, A. R. M.: A mechanistic view of the particulate
1211   biodiffusion coefficient: Step lengths, rest periods and transport directions, J Mar Res, 48, 177–207,
1212   https://doi.org/10.1357/002224090784984560, 1990.

1213 Whitesides, C. J. and Butler, D. R.: Bioturbation by gophers and marmots and its effects on conifer germination,
1214   Earth Surf. Process. Landforms, 41, 2269–2281, https://doi.org/10.1002/esp.4046, 2016.

1215 Wilkinson, M. T., Richards, P. J., and Humphreys, G. S.: Breaking ground: Pedological, geological, and ecological
1216   implications of soil bioturbation, Earth-Science Reviews, 97, 257–272,
1217   https://doi.org/10.1016/j.earscirev.2009.09.005, 2009.

1218 Williams, J. R. (Ed.): Sediment-yield prediction with Universal Equation using runoff energy factor. In Present
1219   and prospective technology for predicting sediment yield and sources: Proceedings of the Sediment-Yield
1220   Workshop, ARS-S-40, United States Department of Agriculture (USDA), New Orleans, USA, 1975.

1221 Wilson, M. F. J., O'Connell, B., Brown, C., Guinan, J. C., and Grehan, A. J.: Multiscale Terrain Analysis of
1222   Multibeam Bathymetry Data for Habitat Mapping on the Continental Slope, Marine Geodesy, 30, 3–35,
1223   https://doi.org/10.1080/01490410701295962, 2007.

1224 Wischmeier, W. and Smith, D. D.: Predicting rainfall erosion losses - A guide to conservation planning,
1225   Agriculture Handbook, 1–58, 1978.

1226 Wood, S. N.: Generalized Additive Models, Chapman and Hall/CRC, 2006.

1227 Wösten, J.H.M. (Ed.): Soil Quality for Crop Production and Ecosystem Health, Developments in Soil Science,
1228   Elsevier, 1997.

1229 Wu, C., Wu, H., Liu, D., Han, G., Zhao, P., and Kang, Y.: Crab bioturbation significantly alters sediment microbial
1230   composition and function in an intertidal marsh, Estuarine, Coastal and Shelf Science, 249, 107116,
1231   https://doi.org/10.1016/j.ecss.2020.107116, 2021.

1232 Yair, A.: Short and long term effects of bioturbation on soil erosion, water resources and soil development in an
1233   arid environment, Geomorphology, 13, 87–99, https://doi.org/10.1016/0169-555X(95)00025-Z, 1995.

1234 Yoo, K. and Mudd, S. M.: Toward process-based modeling of geochemical soil formation across diverse
1235   landforms: A new mathematical framework, Geoderma, 146, 248–260,
1236   https://doi.org/10.1016/j.geoderma.2008.05.029, 2008.

1237 Yoo, K., Amundson, R., Heimsath, A. M., and Dietrich, W. E.: Process-based model linking pocket gopher
1238   (Thomomys bottae) activity to sediment transport and soil thickness, J. Geophys. Res., 33, 917,
1239   https://doi.org/10.1130/G21831.1, 2005.

1240 Yu, C., Zhang, J., Pang, X. P., Wang, Q., Zhou, Y. P., and Guo, Z. G.: Soil disturbance and disturbance intensity:
1241   Response of soil nutrient concentrations of alpine meadow to plateau pika bioturbation in the Qinghai-
1242   Tibetan Plateau, China, Geoderma, 307, 98–106, https://doi.org/10.1016/j.geoderma.2017.07.041, 2017.

1243 Zevenbergen, L. W. and Thorne, C. R.: Quantitative analysis of land surface topography, Earth Surf. Process.
1244   Landforms, 12, 47–56, https://doi.org/10.1002/esp.3290120107, 1987.

1245 Zhang, Q., Li, J., Hu, G., and Zhang, Z.: Bioturbation potential of a macrofaunal community in Bohai Bay,
1246   northern China, Marine pollution bulletin, 140, 281–286, https://doi.org/10.1016/j.marpolbul.2019.01.063, 2019.

1247 Zhang, S., Fang, X., Zhang, J., Yin, F., Zhang, H., Wu, L., and Kitazawa, D.: The Effect of Bioturbation Activity of
1248   the Ark Clam Scapharca subcrenata on the Fluxes of Nutrient Exchange at the Sediment-Water Interface, J.
1249   Ocean Univ. China, 19, 232–240, https://doi.org/10.1007/s11802-020-4112-2, 2020.

1250